Chemosphere 302 (2022) 134823

Contents lists available at ScienceDirect

Chemosphere

journal homepage: www.elsevier.com/locate/chemosphere

Nanocellulose-based sensing platforms for heavy metal ions detection: A comprehensive review

Mahsa Mousavi Langari [a], M. Mirari Antxustegi [b], Jalel Labidi [a,*]

[a] Biorefinery Processes Research Group, Chemical and Environmental Engineering Department, Faculty of Engineering, Gipuzkoa, University of the Basque Country UPV/EHU, Plaza Europa 1, 20018, Donostia, Spain
[b] Biorefinery Processes Research Group, Chemical and Environmental Engineering Department, Faculty of Engineering, Gipuzkoa, University of the Basque Country UPV/EHU, Avenida Otaola 29, 20600, Eibar, Spain

HIGHLIGHTS

- Nanocellulose-based sensors for heavy metal ions detection are presented.
- Optical and electrochemical techniques in heavy metal ions sensors are highlighted.
- Sensing mechanisms involved in heavy metal ions detection is summarized.
- The roles of nanocellulose in heavy metal ions sensors are discussed.

GRAPHICAL ABSTRACT

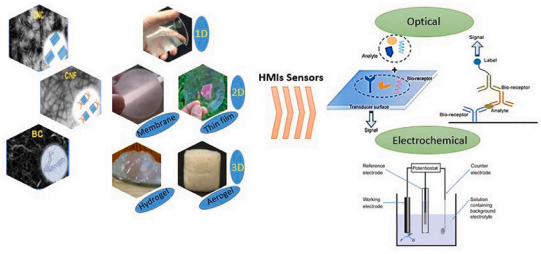

ARTICLE INFO

Handling Editor: Petra Petra Krystek

Keywords:
Nanocellulose
Optical sensor
Electrochemical sensor
HMI
Water

ABSTRACT

Increase in industrial activities has been arising a severe concern about water pollution caused by heavy metal ions (HMIs), such us lead (Pb^{2+}), cadmium (Cd^{2+}) or mercury (Hg^{2+}). The presence of substantial amounts of these ions in the human body is harmful and can cause serious diseases. Hence, the detection of HMIs in water is of great importance. As technological advances have developed, some conventional methods have become obsolete due to some methodological disadvantages, giving way to a second generation that uses novel sensors. Recently, nanocellulose, as a biocompatible material, has drawn a remarkable attraction for developing sensors owing to its extraordinary physical and chemical properties. This review pays a special attention to the different dimensional nanocellulose-based sensors devised for HMIs recognition. What is more, different sensing techniques (optical and electrochemical), sensing mechanisms and the roles of nanocellulose in such sensors are discussed.

1. Introduction

Water is a paramount natural resource on the earth which is being increasingly polluted by industrialization and economic development. HMIs, which are considered extremely toxic elements, are some of the substances contaminating this vital resource via industrial activities. For instance, in the case of metallurgical industries, which includes electroplating metal, mining and smelting, release copper (Cu^{+2}), zinc (Zn^{+2}), nickel (Ni^{+2}), Cd^{+2} and Pb^{+2} (Hasanpour and Hatami, 2020; Ružičková et al., 2018; Yang et al., 2019). Additionally, agricultural

* Corresponding author.
E-mail address: jalel.labidi@ehu.eus (J. Labidi).

https://doi.org/10.1016/j.chemosphere.2022.134823
Received 25 January 2022; Received in revised form 27 April 2022; Accepted 29 April 2022
Available online 4 May 2022

products, mainly manures, fertilizers, pesticides, fungicides and insecticides import Pb^{+2}, Cu^{+2}, Zn^{+2}, Cd^{+2} as well as chromium (Cr^{+3}/Cr^{+6}) into the environment (Briffa et al., 2020; Manzoor, 2020), and paint manufacturing is another remarkable contributor of Pb^{+2}, Zn^{+2} and Cr^{+3}/Cr^{+6} contamination (Lokhande et al., 2011). What is more, Pb^{+2}, Ni^{+2}, Cd^{+2} and also Hg^{+2} are used in several sanitary and cosmetic products, including shower and hair-care products, dyes, shampoos and toothpaste. These HMIs, acting as active ingredients, preservatives or residual contaminants in initial substances like *Aloe vera*, are liberated in waste streams and subsequently in the environment (Ababneh and Al-Momani, 2018). On the other hand, in addition to these mentioned industries, some natural resources, including soil erosion, rainfall and volcano emit ions such as Hg^{+2}, Cu^{+2}, Zn^{+2} and Ni^{+2} into the soil, water and atmosphere (Hasanpour and Hatami, 2020; Manzoor, 2020; Zhao et al., 2017). It is necessary to know that despite the fundamental need of living cells and organisms for small amounts of some HMIs, namely Cu^{+2}, Zn^{+2} and Cr^{+3}, an excessive amount of them in water resources may affect ecosystems and human health adversely. It can be observed that, even if iron ion (Fe^{3+}) plays a vital role in several biochemical reactions, such as respiration, energy metabolism and DNA synthesis, the excessive intake of this element in body causes cancer, Alzheimer or Parkinson (Lesani et al., 2020). On the other hand, there are some other HMIs, such as Ni^{+2}, Pb^{+2}, Cd^{+2} and Hg^{+2} which are extremely poisonous for human body even in very small quantities and cause severe and fatal diseases (Fan et al., 2020; Xu et al., 2020; Zhang et al., 2020a). Hg^{2+} as a kind of pollutant endangers human health and the ecosystem severely because it is highly toxic, persistent and accumulates in the food chain. It brings about renal failure, digestive problems and nerve disorders. This HMI not only exists in coal and some geologic deposits, but also releases into the environment due to anthropogenic processes and the quick growth of industrialization (Balusamy et al., 2020; Fu and Xi, 2020). For these reasons, the amount of HMIs in drinking water must abide by the environmental agencies recommendations, including the US Environmental Protection Agency (EPA), the European Medical Agency (EMA) or the World Health Organization (WHO). Accordingly, HMIs detection in water is a critical matter (Ramdzan et al., 2020). The standard limits of some HMIs, which are determined by mentioned international organizations, alongside their main sources and major detrimental effects are summarized in Table 1.

Conventionally, atomic absorption/emission spectrometry (AAS/AES) (Hasan et al., 2009; Rezvani and Soleymanpour, 2016), X-ray fluorescence spectroscopy (XRF) (Sitko et al., 2015), inductively coupled plasma atomic emission spectrometry (ICP-AES) (Sixto et al., 2016), inductive coupled plasma mass spectrometry (ICP-MS) (Yeung et al., 2017) and atomic fluorescence spectrometry (AFS) (Gómez-Ariza et al., 2005; Li and Guo, 2005) and electrochemical assays (Gumpu et al., 2015) were utilized for HMIs detection. In spite of the immense sensitivity and selectivity of these techniques, they have some drawbacks, including being time-consuming, requiring expensive instruments and skilled operators, and sophisticated sample preparation procedure. Beside these downsides, the huge size of such devices caused them not to be able to be deployed as a portable equipment for on-site monitoring. These disadvantages have led to the advent of more efficient approaches, such as water quality sensors which are selective and sensitive with simple procedure for identifying HMIs in environmental samples (Guo et al., 2019a, 2019b; Huang et al., 2021; Ojha, 2020; Phichi et al., 2020). Overall, sensors are analytical devices employed for recognizing analytes on a basis of biocatalyst sensors, and consist of a receptor, physicochemical signals transducer and a processor for signals interpretation. Depending on the type of the output signals, sensors work based on optical, mechanical, magnetic and electrical principles (Daniyal et al., 2019b; Torres et al., 2020).

Lately, nanomaterials have been broadly investigated for being applied in (bio)sensing applications owing to their unique physicochemical features. However, the toxicological impact of nanomaterials on human health and the environment caused researchers to focus on nanomaterials attained from green resources, mainly polysaccharides, biopolymers and proteins. Among these nano-biomaterials, nanocellulose has exponentially attracted a great deal of attention (Ahankari et al., 2020; Golmohammadi et al., 2017). Nanocellulose is a cellulosic material whose, at least, one dimension is in nano-scale. Nanocellulose is categorized into three types: bacterial cellulose (BC), cellulose nanofibril (CNF) and cellulose nanocrystal (CNC), depending on isolation techniques. The names of the different types of nanocellulose might vary sometimes: BC which is also known as microbial nanocellulose, nanofibrillated cellulose (NFC) might also be referred as microfibrillated cellulose (MFC) or cellulose nanofiber are the names which are attributed to CNF and cellulose nanowhiskers (CNW) or nanocrystalline cellulose (NCC) might be used as alternatives to CNC (Omran et al., 2021;

Table 1
Standard limits of HMIs in drinking water, their main sources and major detrimental effects.

HMI	Standard limits (mg L^{-1})			Sources	Detrimental effects	Ref.
	WHO	EPA	EMA			
Cu^{2+}	1.5	1	3	Electroplating, Cu mining, mineral processing, steel production	Menkes, Parkinson, Alzheimer and Wilson diseases, kidney damage, liver cirrhosis, anemia, intestine irritation, Insomnia	(Balusamy et al., 2020; Hasanpour and Hatami, 2020)
Zn^{2+}	3	5	5	Mining, plating, metallurgy, dust, electroplating	Lethargy, anemia, nervous system disorders, abdominal pain, thirst	Hasanpour and Hatami (2020)
$Cr^{3+/6+}$	0.05	0.1	0.5	Cosmetic raw materials, leather production, tanned leather, industrial pigments, rubbers and ceramics	Gastrointestinal diseases, hepatic encephalopathy, respiratory and cardiovascular problems, renal and endocrine systems defects, hematological, ocular problems	(Balusamy et al., 2020; Hasanpour and Hatami, 2020; Zhang et al., 2020b)
Pb^{2+}	0.05	0.05	0.5	Painting, Pbmining, metal smelting, welding, manufacturing stained glass	Digestive problems, urinary system failure, nervous system damage	(Fu and Xi, 2020; Hasanpour and Hatami, 2020)
Cd^{2+}	0.003	0.005	0.2	Paints, pigments, batteries, plastics and rubbers, engraving process, photoconductors and photovoltaic cells	Anemia, high blood pressure, urinary system toxicity, weight loss, respiratory disease, lymphocytosis, cardiac disease, immune system failure, bone problems	(Hasanpour and Hatami, 2020; Malik et al., 2019)
Ni^{2+}	0.07	0.1	0.1	Coal combustion, diesel and fuel oil burning, tobacco smoking, wind dust, volcano activities, waste incineration, low cost jewelry, stainless steel utensils	Dermatitis, lung fibrosis, asthma, respiratory and cardiovascular diseases, immune system failure, carcinogenic, DNA damage	(Cemple and Nikel, 2006; Genchi et al., 2020; Hasanpour and Hatami, 2020)
Hg^{2+}	0.006	0.002	–	Coal burning, Instrument factory, salt electrolysis, metal smelting, cosmetics	Brain damage, kidney failure	(Kinuthia et al., 2020; Zhang et al., 2020a, 2020b, 2020c)

Raghav et al., 2021). In Fig. 1a-c, the images of various types of nanocellulose, obtained by using electron microscopy, along with their corresponding schematics are depicted.

Generally, nanocellulose is derived from bacteria, marine animals and plants through chemical (e.g. (2,2,6,6-Tetramethyl-piperidin-1-yl)-oxyl (TEMPO) oxidation, acid hydrolysis, and enzymatic reactions), mechanical (e.g. cryocrushing, grinding, high-pressure homogenization, microfluidization and high intensity ultrasonic treatments) and/or biological (e.g. treatment by using bacterial strains like Acetobacter xylinum) approaches (Farooq et al., 2020; Gupta and Shukla, 2020; Piras et al., 2019). In order to isolate the favorable structure and morphology, the aforementioned approaches are deployed consecutively or separately. Nanocellulose isolation can be accomplished via either a bottom-up method from glucose, conducted by bacteria, or a top-down approach from agricultural wastes, plants and crops (Thomas et al., 2020; Tshikovhi et al., 2020).

It should be noted that nanocellulose can be self-assembled into two-dimensional (2D) (e.g., films and membranes) and three-dimensional (3D) products (e.g., aerogels and hydrogels) via hydrogen bonding. Totally, films and membranes, containing nanocellulose are fabricated via filtration or casting, and hydrogels are made through gelation process. The replacement of the liquid component of hydrogel with gas leads to form a low density solid, designated as an aerogel (Hu et al., 2020; Koga et al., 2019; Yuan et al., 2020a, 2020b; Zinge and Kandasubramanian, 2020).

Nanocellulose is used for an assortment of applications from reinforcing components to sensing materials in various scopes, such as curative controls and delivery, nanomedicine as well as environmental conservation. Lately, the utilization of cellulose and its derivatives in HMIs recognition has received an enormous attention of researchers. What make nanocellulose an interesting option for sensing applications are its large surface area, hydrophilicity, superb mechanical and thermal resistance, high crystallinity, facile chemical modification in addition to its biocompatibility, reusability and nontoxicity (Ram et al., 2020; Soriano and Dueñas-Mas, 2018; Teodoro et al., 2019b; Wang et al., 2020b). The modification of nanocellulose can be conducted through introducing particular functional groups to the hydroxyl groups existing on its surface (Fan et al., 2020). Noncovalent surface modification (e.g. oppositely charged groups (Ruiz-Palomero et al., 2016; Zhu et al., 2021)), etherification (Uzuncar et al., 2021), silylation (Cheng et al., 2018), amidation (Riva et al., 2019), esterification (Chen et al., 2019; Tracey et al., 2020), urethanization (Pursula et al., 2018), oxidation (Neubauerova et al., 2020), sulfonation (Dwivedi et al., 2014) and polymer grafting (Anirudhan et al., 2018) are the modifications methods utilized for sensing applications. Nanocellulose plays a significant role as substrate, template, reducing/stabilizing agent, nanofiller and dispersant for immobilizing a variety of metal NPs, plasmonic NPs, photoluminescent and conductive (nano)materials, carbon-based nanomaterials, and fluorescent (bio)molecules in HMIs sensors. Such organic/inorganic hybrid platforms demonstrate exceptional optical and electrical properties (Teodoro et al., 2019b, 2019a; Wang et al., 2020a; Yue et al., 2021). Herein, we have summarized the latest studies conducted on different dimensional HMIs sensors which contain nanocellulose. The roles of nanocellulose in optical and electrochemical sensing are highlighted as well.

2. One-dimensional (1D) nanocellulose-based sensors

1D nanomaterials possess extraordinary features, namely light weight, high sensitivity and transparency, low thickness, low cost, potential for fabricating spacious area as well as excellent mechanical, optical and electrical properties owing to their great aspect ratio. Hence, nanocellulose is a kind of 1D nanomaterial that thanks to its biodegradability has been increasingly attracting a great amount of attention for the development of bio-based materials and nanocomposites, such as sensors (Brett et al., 2019; Gong and Cheng, 2017).

2.1. Optical sensors

Optical sensors are cost effective, highly precise and rapid with the capability of remote, real-time and multiplexed sensing. More importantly, they have less complicated setup for obtaining data and working in comparison to other sensors. Fundamentally, these types of sensors need a diagnosis element to interact with particular analytes which leads the sensor to diagnose the signal engendered by binding event (Daniyal et al., 2019b; Ramdzan et al., 2020; Zhang et al., 2020a, 2020b, 2020c). In detail, optical sensors are composed of four parts: 1) the diagnosis element, where the interaction and the recognition of the analyte occur; 2) the transducer element which is responsible for the conversion of the diagnosis process into a quantifiable optical signal; 3) an optical equipment (process unit) consisting of a light source and 4) a detector which amplifies the primary signal, transmits the alteration of optical signals into a readout unit and identifies it (Mayr and Wolfbeis, 2002). Optical sensors function on a basis of two classifications of detection

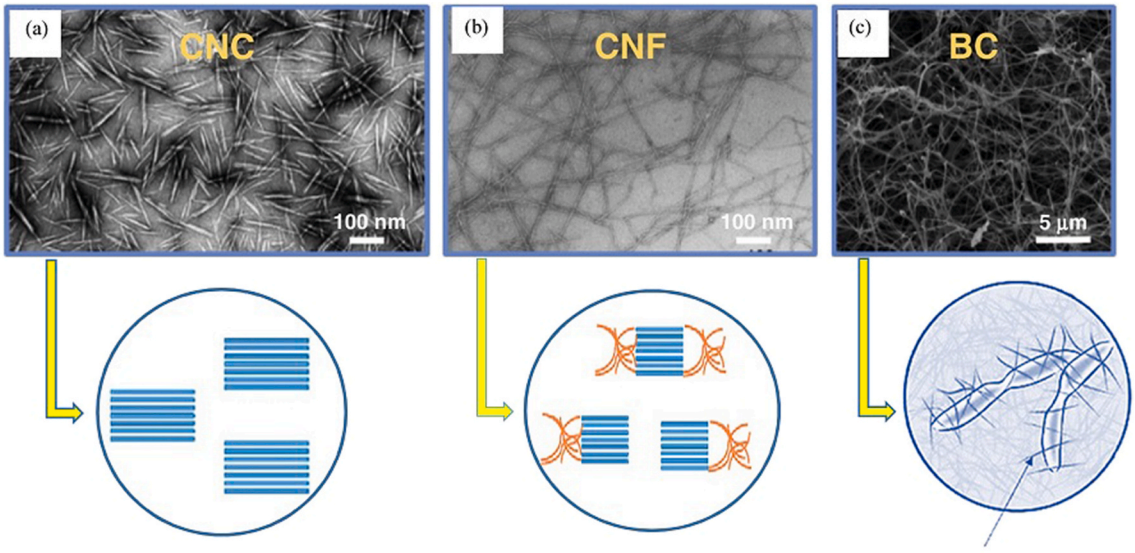

Fig. 1. Transmission Electron Microscopy (TEM) images of CNC (a) and CNF (b) Scanning Electron Microscopy (SEM) image of BC and their corresponding schematics (shown by an arrow) (Abitbol et al., 2016; Piras et al., 2019).

procedures: label-based detection and label-free detection. What is referred to as a label is a foreign substance which is attached to the target molecule temporarily or chemically via a label processing. The label-based sensors work based on colorimetric, fluorescence and luminescence techniques (Aliheidari et al., 2019; Ivanova et al., 2016; Khansili et al., 2018). The schematic of a kind of label-free and label-based biosensors is depicted in Fig. 2a, b, respectively. Although label-based sensors are quite sensitive and benefit from a low detection limit even for one single molecule in cell and molecular biology, they have some downsides. As a case in point, in fluorescent-based sensors, fluorescent tags are also likely change the properties of host molecules during labeling process. Moreover, fluorescence signal bias may disrupt quantitative analysis since it is not conceivable to control the number of fluorescent substances on each host molecules efficiently. Consecutively, quantitative detection necessitates relatively high price photonic devices. Overall, label-based sensors assemblies require additional step for labeling which consumes additional time and reagents. (Fan et al., 2008; Zhu et al., 2010). In contrary to label-based sensors, label-free ones provide facile and low cost diagnosis as target analytes need not get labeled or changed, and are recognized in their natural and unmodified forms. Another interesting feature of this type of sensors is the capability of analyzing the kinetic and thermodynamic of molecular interaction quantitatively (Sang et al., 2016). Optical label-free sensors function on a foundation of various detection mechanisms, including absorption, refractive index, light polarization and Raman spectroscopy, resulting in colorimetric, fluorescence, luminescence, surface plasmon resonance (SPR) and surface enhanced raman scattering (SERS) sensors (Fan et al., 2008; Golmohammadi et al., 2017; Mayr and Wolfbeis, 2002). What is more, some kinds of materials could be exploited as recognition units in optical label-free sensors thereby acting as both colorimetric reporter and fluorescence quencher, thus lead to the fabrication of dual-signal sensors (Yan et al., 2014).

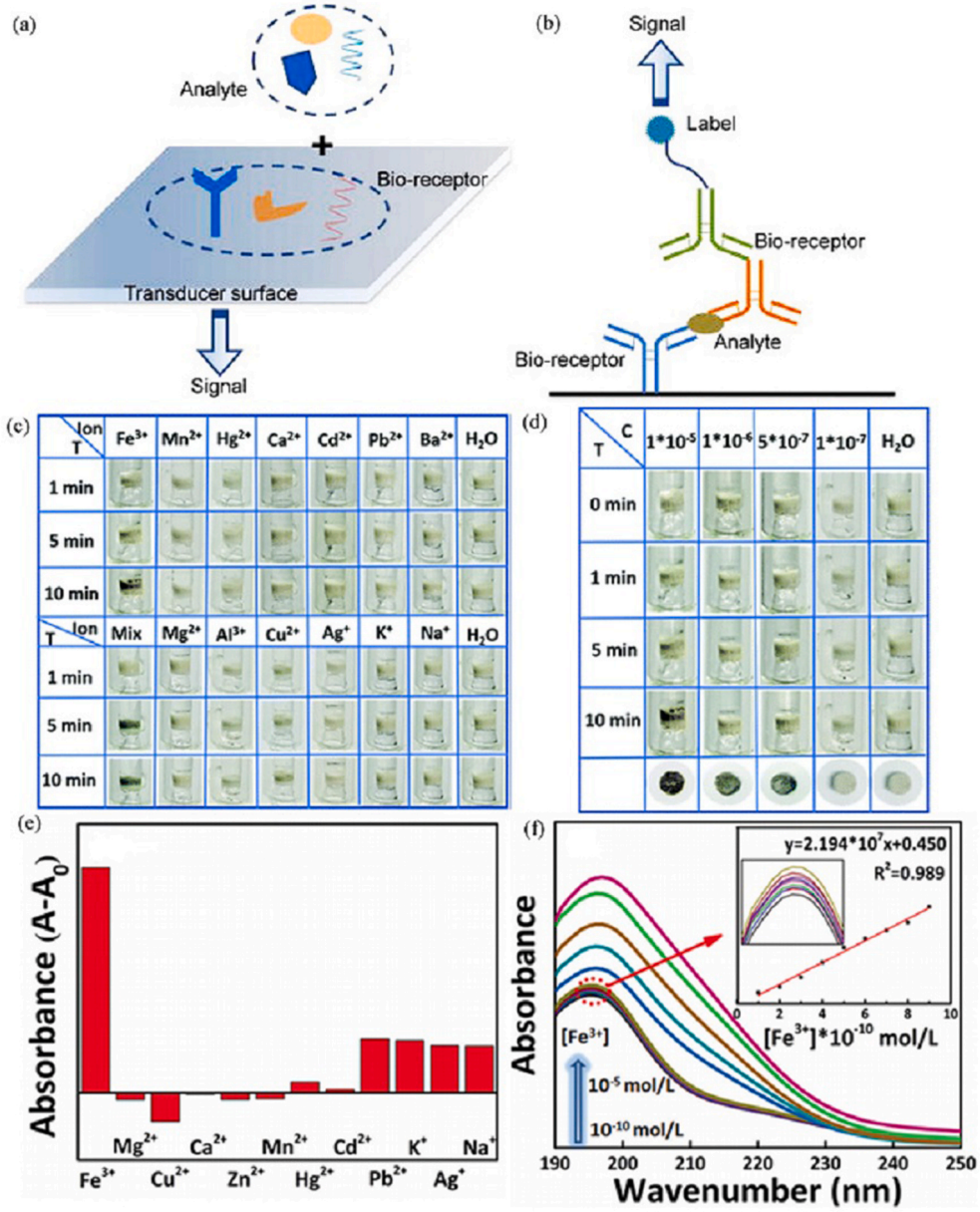

Fig. 2. Schematic of a type of a) label-free and b) label-based biosensors (Ivanova et al., 2016). c) Selectivity of the solid TOCNF-DA towards Fe^{3+} (among various HMIs) as a colorimetric sensor and d) the relevant LOD, e) detection of Fe^{3+} by means of the aqueous TOCNF-DA solution and f) the corresponding LOD (Wang et al., 2020b).

2.1.1. Fluorescence sensors

Normally, one or more fluorescent substances are attached to receptors in order for manufacturing fluorescent sensors. The interaction between the receptor and a specific analyte caused the transduction of a fluorescent signal which can be further detected readily (Sarma et al., 2019). The more the number of analytes, the more intense the fluorescent signal (Fan et al., 2008). On the other hand, natural polymers, such as cellulose are widely regarded as matrix/carrier for the immobilization of dyes as fluorescent substances. Three polar OH groups existing on the surface of cellulose provide several sites for creating hydrogen bonding between the polar groups of dye molecules and ions (Jiang et al., 2020; Zhang et al., 2020a). Accordingly, Song et al. (2019) created dye-labeled TEMPO-oxidized CNC (TOCNC) by means of binding 4-((2-amnioethyl) amino)-9- methyl-1,8- naphthalimide (AANI) dye on CNC for detecting Pb^{2+}. In this work, the detection of Pb^{2+} occurred through the complexation of this HMI with dye groups and carboxyl groups on TOCNC. Zhang et al. (2012) developed a sensor discriminating Fe^{3+} in the aqueous solution of Fe^{2+} and other HMIs. For this reason, they modified CNC with a pyrene (Py) fluorophore resulted in the enhancement of the Py emission. The recognition of Fe^{3+} occurred via the electron transfer between redox active HMIs and the excited Py, the complexation of them with Py, which was proved by Benesi–Hildebrand equation and Sterm-Volmer plot, and fluorescent quenching. Recent years have witnessed the application of fluorescent probe in HMIs detection. For materials without intrinsic fluorescence characteristics, such as nanocellulose, fluorescent complex formation, derivatization and fluorescence quenching can be operated as indirect fluorometric methods. Among named methods, fluorescence quenching is the most reported probe for Fe^{3+} recognition (Karuk Elmas et al., 2020; Li et al., 2020).

2.1.2. SPR sensors

SPR is the resonant oscillation of conduction electrons at the interface between metal and dielectric material which is stimulated by incident light. When resonance happens, the reflected light is quenched. SPR, as a complementary optical method, has attracted many researchers' attention to build a sensor through incorporating an active layer with it. The sensitivity and detection limit of the sensor can be determined on a foundation of SPR responses to target metal ions concentrations (Ramdzan et al., 2020; Zhu et al., 2020). Migliorini et al. (2020) functionalized CNW with gold nanoparticles (AuNP) so as to establish a simple nanocomposite (CNW/AuNP) recognizing Cd^{2+} in real sample, in the existence of interfering HMIs with 60 nM limit of detection (LOD). The cluster of AuNP formed via binding citrate anions on its surface to Cd^{2+}, contributed to the optical change in SPR band. The increase in Cd^{2+} concentration in the range of 500–2000 nM decreased the absorbance linearly.

2.1.3. Dual-signal sensors

Colorimetric detectors, functioning through change in its color which can be observed with naked eyes, demonstrate substantial advantages over other analytical methods in terms of their selectivity and sensitivity, simplicity and detection limit (Migliorini et al., 2020). Ram et al. (2020) devised a spherical nanocellulose-based (SNC) sensor which was selective to Cu^{2+} and tolerant to pH in a range of 3–10. In this work, two kinds of modifications on SNC were performed using Schiff-base formation, with diethylenetriamine (DETA) and ethanolamine (EA), leading to the production of SNC-DETA and SNC-DETA-EA composites, respectively. SNS-DETA just had a colorimetric sensing in high concentrations (100–150 mg L^{-1}) unlike SNC-DETA-EA, which turned into dark blue from light blue at 0.5–100 mg L^{-1} concentrations. This color alteration was justified by internal charge transfer between ligand moieties, mainly ester, primary and secondary amine, imine, and empty d-orbital of Cu^{2+}. However, both sensing composites showed fluorescent detection as well. Another colorimetric and fluorescent sensor, capable of detecting Hg^{2+}, was produced by Ye et al. (2020) In this work, acting as a sensor, Rhodamine B (RhB) labeled CNC responded to Hg^{2+} in pH = 3–12 via changing in its color (red) and fluorescence emission (orange). The complex formed through binding RhB–CNC with Hg^{2+} was conducive to this color change. The Benesi–Hildebrand plot was used for the calculation of binding constant in this complex (4.15 × 105 M) and binding stoichiometry (1:1). Rhodamine derivatives, which were utilized for the first time in 1997 by Czarnik, have drawn many researchers' attention recently (Bergmann, 1932). Wang et al. (Wang et al., 2020b) grafted dopamine (DA) onto TOCNF via amidation in order to devise a polymorphic sensor (TOCNF-DA) diagnosing Fe^{3+} in the mixture of various HMIs. The detection occurred because Fe^{3+} interacted with amid and phenolic hydroxyl groups of TOCNF-DA. In this process, a stable compound was formed through the chelation of Fe^{3+} by nitrogen and oxygen. This sensor showed high selectivity and sensitivity in the both forms of solid and aqueous solution by changing in color from white to dark green in less than 10 min (LOD = 5×10^{-7} M) (Fig. 2c, d) and ultraviolet–visible (UV-VIS) spectrophotometry (LOD = 6.6×10^{-11} M) (Fig. 2e, f), respectively.

3. 2D nanocellulose-based sensors

2D nanocellulose-based composites are generally divided into self-standing or supported films, which can be in the forms of coatings on bulk materials and free-standing membranes (Bacakova et al., 2020). 2D nanocellulose-based platforms have been widely investigated to eliminate the disadvantages of the conventional substrates, mainly high surface roughness and low mechanical strength in aqueous medium, for manufacturing sensing materials (Soriano and Dueñas-Mas, 2018).

3.1. Optical sensors

3.1.1. Fluorescence sensors

Carbon quantum dots (CQDs) are a type of fluorescent functional nanomaterials which is prepared via a simple hydrothermal method and shows low toxicity and high luminous purity (Zhang et al., 2020c). Xue et al. (2020) developed Fe^{3+} sensor based on CQDs in which TOCNF was applied as a substrate. The covalent bonding between the carboxyl of TOCNF and the amino groups of CQDs prevented CQDs from aggregation and led to the highly transparent and photoluminescent nanopaper. What is more, this nanopaper presented excellent thermal and mechanical stability. In comparison to recent fluorescent sensors established based on carbon for Fe^{3+} recognition, the obtained nanopaper showed decent sensitivity to Fe^{3+} as a fluorescent sensor. Lv et al. (2017) manufactured a membrane probe recognizing Fe^{3+} in aqueous media. They incorporated nitrogen doped CQDs (N-CQDs), synthesized using ethanediamine (EDA) and citric acid (CA) as precursors through hydrothermal method, into culture media for the first time. The resultant composite membrane BC/NCQDs was able to detect Fe^{3+} in the range of 0.5–600 μM with 84 μM LOD. Later, they manufactured another Fe^{3+} detector through the method similar to their previous study, yet in this work, they applied graphene oxide QDs (N-GOQDs) instead of CQDs. In recent years, GOQDs has drawn remarkable attention in biosensing owing to its astounding physicochemical, optical, photoluminescence properties, whose surface functionality changes, including heteroatom doping, and structural defects can influence these properties (Khan and Patil, 2020). The obtained sensor (BC/NGOQDs) was investigated in terms of its selectivity to variant HMIs in pure water and its sensitivity to various concentrations of Fe^{3+}. Fluorescent spectra of the sensor quenched by Fe^{3+}, and the fluorescent intensity dwindled by increase in Fe^{3+} concentration. The quenching occurred because of the complex which was produced by robust coordination of Fe^{3+} with primary amine and hydroxyl groups. This sensor was able to detect Fe^{3+} in both ultrapure water and real water samples and indicated favorable reproducibility through washing with ethylenediamine tetraacetic acid (EDTA). At the end, the performance of developed sensor in the

detection of Fe^{3+} in lake water was compared with the conventional method, inductively coupled plasma mass spectrometry (ICP-MS). Both methods showed approximately the same amount, proving the fact that the manufactured sensor would be a promising tool for determining Fe^{3+} even in lake water (Lv et al., 2019).

Another fluorescent sensor was prepared by Wang et al. (Wang et al., 2020b) which was able to detect Cu^{2+} in a wide range of pH from 3 to 11. They synthesized europium metal-organic framework (Eu-MOF) on the surface of TOCNF in ethanol/water medium. The abundance of hydroxyl group on TOCNF contributed to Eu^{3+} adsorption and ultimately Eu-MOF growth on it in the form of film or NPs. TOCNF prevented Eu-MOF from agglomeration by diminishing its particle size and caused it to grow in different direction. With regard to the results obtained from the evaluation of sensing performance in the existence of variant Cu^{2+} concentrations, fluorescence intensity showed a linear relationship with Cu^{2+} concentrations. It can be concluded that Eu-MOF@TOCNF was an ultimate sensor for recognizing Cu^{2+} in complex water system and water body. There are some other nanocellulose-based sensors which were capable to sense Cu^{2+} alongside other HMIs. As a case in point, Rahmawati et al. (2020) prepared the portable, reusable and fast responsive sensor film for recognizing both Cu^{2+} and cesium (Cs^{+}). However, it was more sensitive towards Cu^{2+} with wider detection range. This sensor was manufactured via the chemical immobilization of a tetradentate ligand (3,5-bis(((2- hydroxynaphthalen-1-yl) methylene) amino) benzoic acid) (3,5-BHNMABA) on TOCNF. Subsequently, it deposited on glass substrate. This study paved the way for radioactive waste treatment.

3.1.2. SPR sensors

The integration of CNC and GO are deployed to fabricate SPR sensors for Cu^{2+} diagnosis owing to the great electrical and optical features of GO (Daniyal et al., 2018a).

Daniyal et al. (2018b) developed a sensor where CNC had been hydrophobized using hexadecyl trimethyl ammonium bromide (CTA) before integrating it with GO. Afterwards, CTA-CNC/GO nanocomposite was deposited on a gold layer which had been spin coated onto a glass substrate. They investigated its sensing performance and characteristics in two distinct works. Fig. 3a depicts the schematic of SPR setup utilized in both these works. In the former, the characterization of obtained sensor showed the produced functional groups attached to the surface of CNC, its homogeneity and high absorption of the nanocomposite. Besides, the diagnosis of Cu^{2+} was conducted by SPR spectroscopy by injecting different concentrations of Cu^{2+} (from 0.01 mg L^{-1} to 0.5 mg L^{-1}) in the hollow and recording the reflected beam. This sensor was able to diagnose the concentration of Cu^{2+} as low as 0.01 mg L^{-1}. In the latter, they collected resonance angles (SPR curves) for a wider range of Cu^{2+} concentrations (from 0.01 mg L^{-1} to 60 mg L^{-1}). As illustrated in Fig. 3b, the SPR curves for the Cu^{2+} concentrations shifted little by little because of the formation of shared electrons between Cu^{2+} and CNC with negative charges on its surface. Conversely, as can be observed in Fig. 3c, for Cu^{2+} concentrations more than 0.5 mg L^{-1}, SPR curves were the same as one another inasmuch as the surface of sensing platform was literally covered with Cu^{2+}. According to Fig. 3d, the plot of SPR curves fitted Langmuir model with the constant of 4.075×10^3 M for binding affinity. Furthermore, the sensitivity of the resultant sensor towards Cu^{2+}, shown in Fig. 3e, calculated 3.271 L mg^{-1} in the aqueous solutions containing low concentrations of Cu^{2+} (0.01–0.1 mg L^{-1}). This sensor was examined for detecting Ni^{2+} in another study, and results exhibited that the sensor had better performance for Cu^{2+} detection. Although capable to recognize 0.01 mg L^{-1} concentration of Ni^{2+} as well as Cu^{2+}, it identified Ni^{2+} in a range of 0.01–0.1 mg L^{-1}, which was wider in case of Cu^{2+} (0.01–0.5 mg L^{-1}). It is noteworthy to mention that the constant of binding affinity and sensitivity towards Ni^{2+} were reported 1.62×10^3 M and 1.509° L mg^{-1}, respectively, which were lower for Cu^{2+} detection (Daniyal et al., 2018a, 2019a). This platform was also able to recognize Zn^{2+} at the low concentration of 0.01 mg L^{-1} (Daniyal et al., 2019b). Later, they went on to establish another SPR sensor through the incorporation of GO with unmodified CNC for the purpose of identifying Cu^{2+} and Zn^{2+} at 0.01, 0.1, and 1 mg L^{-1}. Fig. 3f, g exhibit the structures of CNC-GO before and after being in exposure to Cu^{2+}, respectively. The interaction of these metal ions with this sensor, occurs because of the existence of $-COO^{-}$ or SO_3^{-} functional groups, and it was characterized with X-ray photoelectron spectroscopy (XPS) after employing the SPR technique (Daniyal et al., 2020).

3.1.3. Colorimetric sensors

Milindanuth et al. (Milindanuth and Pisitsak, 2018) manufactured a sensor based on RhB treated BC. Herein, RhB, as a colorless substance selective to Cu^{2+}, was turned into pink when subjected to the aqueous solution containing Cu^{2+} along with barium (Ba^{2+}), Cr^{2+}, Cd^{2+}, Zn^{2+}, Co^{2+}, Mg^{2+}, Hg^{2+}, manganese (Mn^{2+}), Pb^{2+} and tin (Sn^{2+}). The most intense color alteration was observed at pH = 6 since the carbonyl group existing in the spirolactam ring was protonated by Cu^{2+}, which was resulted in the RhB ring opening and color change. In this study, the comparison between the performance of sensors where BC and cellulosic paper applied as substrates revealed the superiority of BC. Because of its higher porosity and vaster surface area, the color intensity of the BC-based sensor in response to Cu^{2+} was more visible.

3.2. Electrochemical sensors

Recently, electrochemical techniques have attracted a huge amount of attention owing to their sensitivity, rapidity and ability for reaching more satisfactory quantitative results in the realm of HMIs detection (Shen et al., 2017). Electrochemical sensors are capable of recognizing both electrochemical and electrical signals. These signals are created by the charge transfer among sensing probes and target molecules. According to the equation (1), *o* can be reduced into *r*, or *r* can be oxidized into *o*, and there will be an equilibrium between *o* and *r* in their oxidized (o^{n+1}) and reduced forms (r^{n}), respectively, which produces the stream of electrons (Islam and Channon, 2019).

$$r^{n} \leftrightarrow o^{n+1} + e^{-} \quad (1)$$

Fig. 4a illustrates the most efficient cell assembly of electrochemical sensors and the charge transfer occurring in it. This electrolytic cell consists of three electrodes, namely reference electrode (RE), working electrode (WE) and counter electrode (CE) (Islam and Channon, 2019; Sarma et al., 2019). Generally, electrochemical sensors are divided into potentiometric, amperometric/voltammetric, impedimetric and conductometric which measure oxidation/or reduction potential, electrical current, electrical conductance and impedance, respectively (Shetti et al., 2018; Torres et al., 2020; Yoon et al., 2020).

3.2.1. Voltammetric sensors

Voltammetric sensors are types of sensors that work on the foundation of measuring a current flow in WE, which is placed in an electroactive solution, at different potentials. Generally, various kinds of electrodes, such as glassy carbon electrode (GCE), pencil graphite electrode (PGE), carbon paste electrode (CPE) or gold and platinum electrodes are utilized as WEs. The aforementioned electrodes require to be modified so as to recognize variant HMIs specifically (Chillawar et al., 2015). There are different types of voltammetry techniques, including cyclic voltammetry (CV), differential pulse voltammetry (DPV), linear sweep voltammetry (LSV) and square wave voltammetry (SWV) whose differences are in the forms of time wave engendered by the corresponding functional application (Lu et al., 2018). As a case in point, Sakwises et al. (2017) employed CV measurements for determining the correspondence between applied potential and current signals for detecting Ni^{2+} in an acidic aqueous media. In this work, Ag/AgCl, paper-based composite and Pt-wire were the three electrodes of RE, WE and CE, respectively. This paper-based composite was developed by

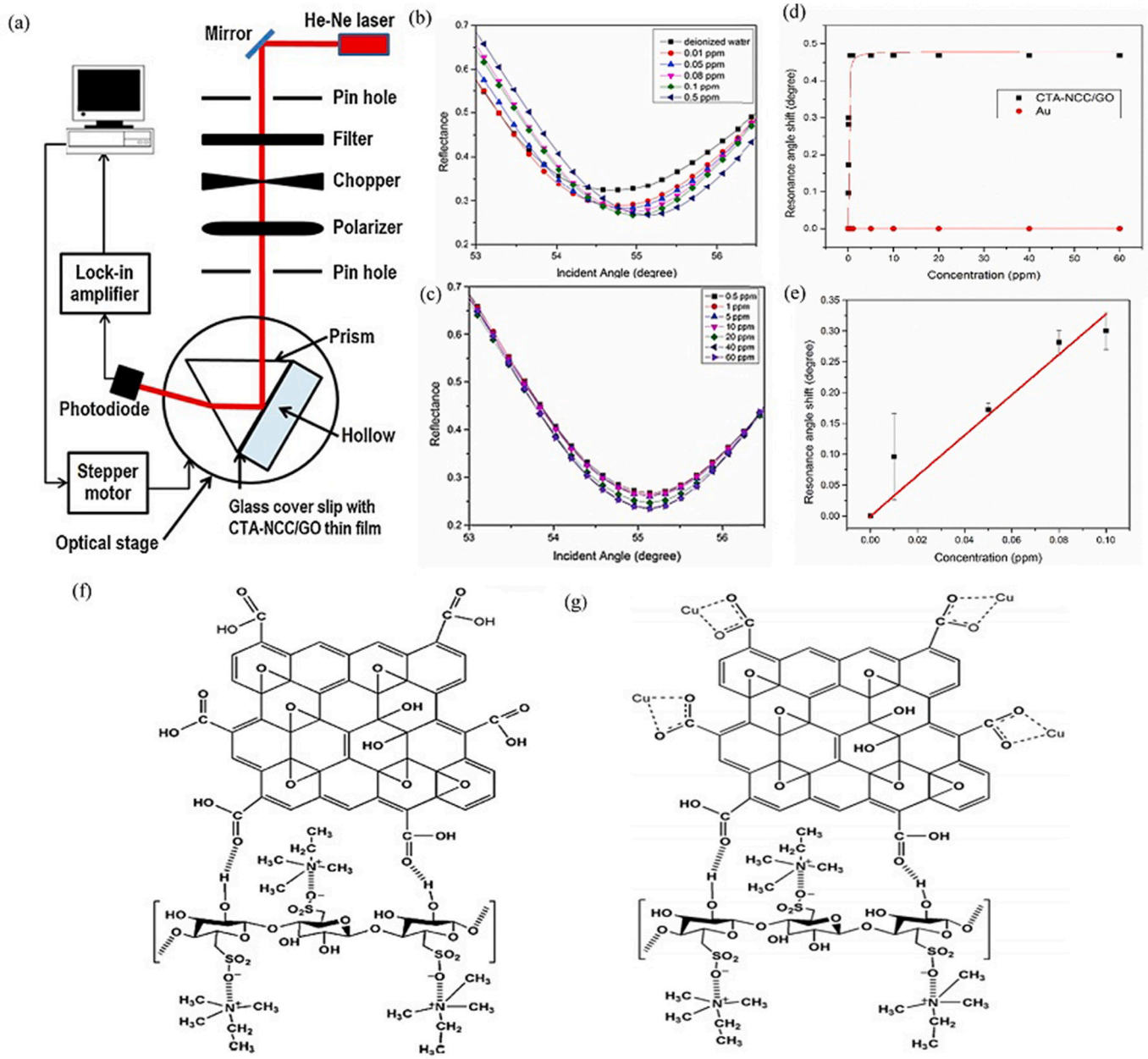

Fig. 3. a) Schematic of SPR setup. SPR curves of the sensor in contact with Cu^{2+}, b) 0.01–0.5 mg L^{-1} and c) 0.5–60 mg L^{-1}. d) Langmuir isotherm model for SPR curves shift ascribed to sensing platform and gold in contact with Cu^{2+}. e) SPR curves shift of sensing platform in contact with 0.01–0.1 mg L^{-1} Cu^{2+} (Daniyal et al., 2018a). Schematic of f) CTA-CNC/GO structure and g) possible interaction between CTA-CNC/GO and Cu^{2+} (Daniyal et al., 2020). (For interpretation of the references to color in this figure legend, the reader is referred to the Web version of this article.)

embedding SnO_2 into BC matrix. Ni^{2+} caused electrons to transfer in the interface of electrode and solution and increased conductivity which made it detectable. Zinoubi et al. (2017) modified GCE with NFC film, acted as a matrix, via simple adsorption aiming to devise a sensor tracing Cd^{2+}, Cu^{2+}, Pb^{2+} and Hg^{2+} in seawater samples by using DPV. They optimized the operational conditions, namely, deposition time and potential, accumulation time, and electrolyte pH to acquire the most sensitive NFC matrix and low detection limit (0.5 nM). What is more, they washed the NFC film with EDTA for the removal of adsorbed HMIs and regenerating it. Among others, the resultant sensor showed more sensitivity and lower LOD for Cu^{2+} due to its high affinity to the NFC film. Another sensor which was capable of detecting Cu^{2+} was suggested by Taheri et al. (2018). They modified PGE with D-penicillamine anchored nanocellulose (DPA-NC) (Fig. 4b, c), and employed SWV technique to recognize this HMI in both tap and river water in pM concentration. This modification increased the SWV responses because of the nanocellulose porous structure alongside the complex formation between the groups containing oxygen or nitrogen in DPA-NC and Cu^{2+}. To calculate the LOD of Cu^{2+}, the modified electrode immersed in variant concentrations of Cu^{2+} (0–100 pM), and the SWV responses was measured (Fig. 4d). The sensitivity and LOD of the DPA-NC/PEG were measured 0.2 μA $(pM)^{-1}$ and 0.048 pM, respectively. The obtained sensor was reusable and could be regenerated by exerting the potential of 0.6 V in nitrate solution (pH = 2, T = 120 s) causing Cu^{2+} removal. Qin et al. (2018) modified GCE with γ-AlOOH-carbonated BC (γ-AlOOH-CBC), and applied DPV for recognizing Cd^{2+} and Pb^{2+} in drinking water. In this work, they fabricated γ-AlOOH-CBC via pyrolysis and hydrothermal methods in which CBC was utilized as a carrier for growing γ-AlOOH on its surface. The superb conductivity and the high adsorption of γ-AlOOH led to the satisfactory selectivity and sensitivity

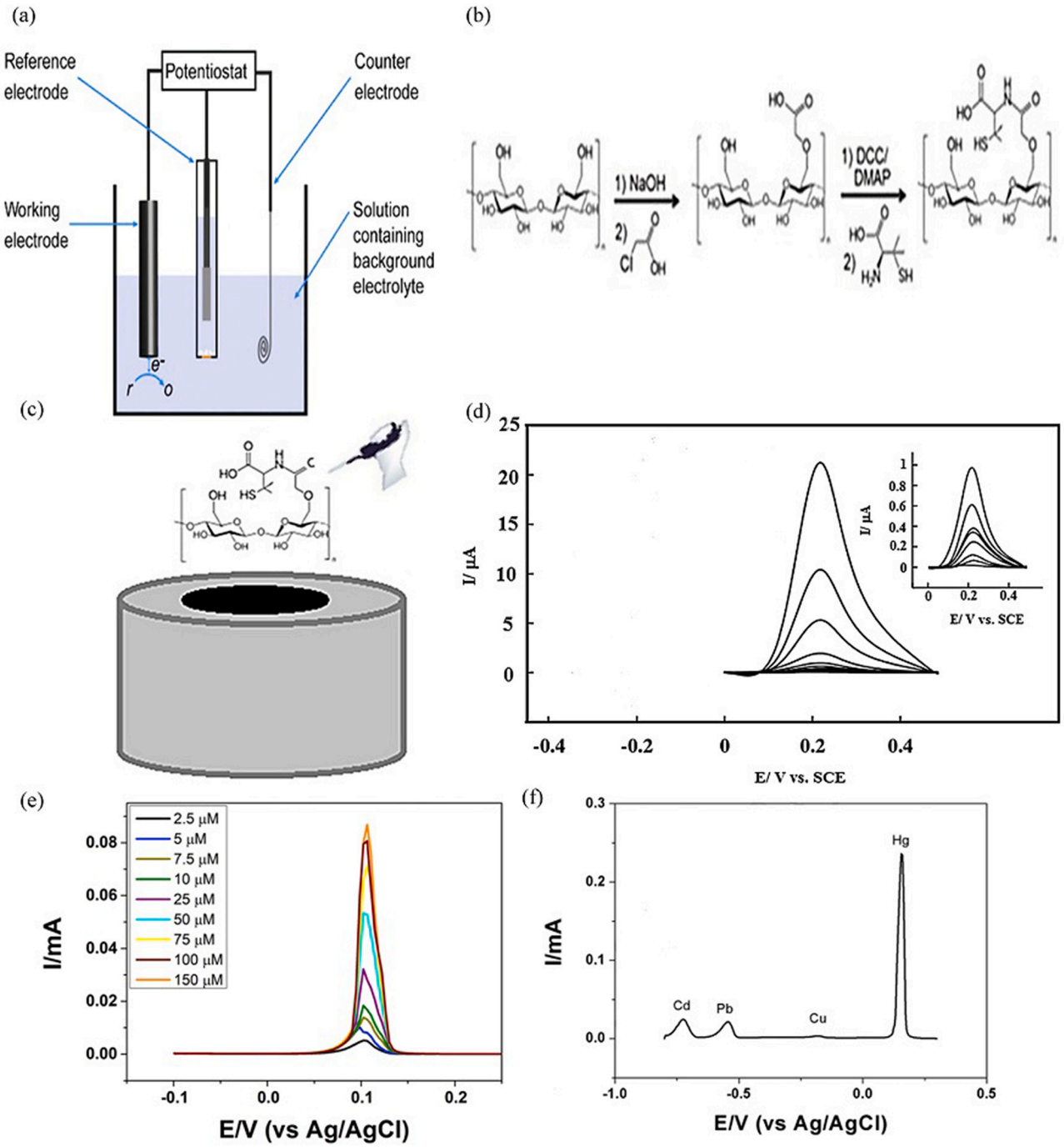

Fig. 4. a) Schematic of a three-electrode electrochemical sensor with charge transfer mechanism (Islam and Channon, 2019). b) DPA-NC synthesis. c) The modification of PEG with DPA-NC. d) SWV curves of DPA-nanocellulose/PEG after immersing in different concentrations of Cu^{2+} (0–100 pM) (inset: SWV in the range of 0–4.5 pM concentrations (Taheri et al., 2018). DPV curves of PA6/CNW/rGO after immersing e) in different concentrations of $Hg^{2+}$and f) in the mixture of Cu^{2+}, Pb^{2+}, Cd^{2+} and Hg^{2+} (Teodoro et al., 2019a).

for the mentioned HMIs detection. The LOD for Cd^{2+} and Pb^{2+} were 0.17 µg L^{-1} and 0.1 µg L^{-1} respectively.

The results obtained from the γ-AlOOH-CBC/GCE performance was consistent with the outcomes attained from ICP-MS. Teodoro et al. (2019a) devised a novel electrochemical sensor with low LOD (0.0052 µM) and broad dynamic linear range (2.5–200 µM) for detecting Hg^{2+} in real samples from river water to tap water. This sensing platform was based on CNW/rGO hybrid system, increasing the charge transfer, and (polyamide 6) PA6 electrospun nanofibers as a Hg^{2+} sensing element. The sensitivity and selectivity of the sensor towards Hg^{2+} was determined by investigating its performance in various concentrations of Hg^{2+} and in the presence of Cu^{2+}, Pb^{2+}, Cd^{2+} by using DPV (Fig. 4e, f). In this platform, CNW acted as a reducing agent for rGO whose action was proved by fourier transform infrared (FTIR) and UV-VIS spectroscopies.

3.2.2. *Impedimetric sensors*

Functioning on a basis of changes in impedance at the surface of sensor after interacting with target analytes, electrochemical impedance spectroscopy (EIS) technique is exploited in the impedimetric method. To sum up, in this method, the exertion of small sinusoidal perturbation to elechtrochemical system generates sinusoidal signal. Generally, after

applying AC potential in a specific range of frequency, the engendered current is collected by using potentiostat. Since these measurements produce a great deal of data, visual analysis is not conceivable, and multivariate data analysis is required so as to simplify data visualization. The impedance data, as a result, is interpreted through modelling the data to a proper electrical circuit which consists of capacitors, inductors and resistors (Fiel et al., 2019; Teodoro et al., 2019b). In this case, regarded as the array of nonspecific sensors, electronic tongues (E−tongue) with the capability of analyzing complex liquids are employed. The array engenders signals which can be ascribed to special qualities or properties of the specimens by means of an appropriate software. Normally, their responds toward samples is qualitative, and in some cases, it can determine the concentration of one analyte in the sample. In summary, the performance of E−tongue is based on two different parts; The former is that it consists of the array of sensors, and the latter is data processing methods (Rodríguez-Méndez et al., 2010). An efficient approach for statistic interpretation of data is the utilization of multivariate data analyses, including principal components analysis (PCA), linear discriminant analysis (LDA), partial least square (PLS) regression, artificial neural network (ANN) (Geană et al., 2020). Teodoro et al. (2019b) succeeded to use E−tongue for establishing a kind of impedimetric sensor for identifying different HMIs (Cd^{2+}, Cu^{2+}, Ni^{2+} and Pb^{2+}). For this reason, they prepared several sensing units through distinct combinations of PA6 electrospun nanofibers, CNW and silver nanoparticles and deposited them on gold interdigitated electrodes (IDEs) surface to be utilized as sensing probes of an E−tongue (((PA6/CNW:Ag)$_{bulk}$[1]/IDE, (PA6)$_{im.CNW:Ag}$[2]/IDE and (PA6/CNW)$_{im.Ag}$[3]/IDE)). The proposed units, except the ones composed of solely PA6 or PA6 and CNW, were able to discriminate different heavy metal ionic solutions at the concentration of 1 mmol L^{-1}. To be more exact, the ones containing hybrid CNW: Ag improved the classification of mentioned solutions. After opting for the sensing probes, it was feasible to categorize the different concentrations of aqueous solution contaminated with Pb^{2+}. In addition, they could distinguish pure water from Pb^{2+}aqueous solution at minimum concentration of 10 nmol L^{-1}.

4. 3D nanocellulose-based sensors

3D macroscopic matrixes of nanocellulose structures are represented by hydrogels and aerogels (Bacakova et al., 2019). Hydrogels are prepared via the removal of water during the conversion of cellulose to nanocellulose, and aerogels are produced from hydrogel or dispersion, further dried by means of various methods, including supercritical, convective or freezing-based ones. Carlsson et al. (2012) produced conductive CNF aerogels through polymerizing pyrrole onto TOCNF chemically, subsequently dried by supercritical CO_2 drying, ambient drying and freeze drying (De France et al., 2020; Muhd Julkapli and Bagheri, 2017).

4.1. Optical sensors

Several studies have been undertaken on establishing 3D nanocellulose-based sensors (hydrogels and aerogels) which solely function on a foundation of fluorescent technique. Some of them are described subsequently. Mohammed et al. (2016) developed a hydrogel which was used for sensing and adsorbing Hg^{2+} at the same time. In this sensor, CNC was applied as a substrate for bovine serum albumin (BSA) protected Au nanoclusters (Au@BSA NCs) in the presence of alginate (ALG). Au@BSA NCs intensified the luminescence properties during the process of detection. The strong metallophilic interaction between Au^{2+} and Hg^{2+} on the surface of Au@BSA NCs quenched the fluorescence of nanocomposite completely and made it a competent sensor for Hg^{2+} recognition. However, it suffered from a flaw which was the lack of reusability, since the fluorescence properties of Au@BSA NCs could not be recovered after binding to Hg^{2+}. Later, Lei et al. (2021) used the combination of BSA-Au NCs and TOCNC aimed at designing a sensor and adsorbent selective to Hg^{2+}. The mechanism of adsorption was justified through the complexation interaction between Hg^{2+} with amino groups, the electrostatic attraction of Hg^{2+} with carbonyl and hydroxyl groups in addition to metallophilic interaction of Hg^{2+} with Au^{+}. In this work, the reported LOD and linear range of detection were respectively 2.7 mg L^{-1} and 5–150 mg L^{-1}. Yue et al. (2021) produced a kind of hydrogel via the in situ polymerization of TOCNF/salicylaldehyde thiosemicarbazone (ST) in the matrix of PVA/borax which was able to sense Cu^{2+}. The utilization of TOCNF caused ST (fluorescent material) to disperse homogenously throughout the PVA/borax matrix and enhanced the mechanical properties of matrix by 2.66 times. Sensing strategy of this sensor was explained through forming the complex between Cu^{2+} and TOCNF/ST, culminated in quenching fluorescent. The higher the concentration of Cu^{2+}, the lower the fluorescence intensity. The LOD of the sensing platform at 485 nm was 0.086 μM. It is notable that the formation of O–B–O bond between diol unit and borate ion on the surface of PVA made it thermally reversible, which led it to get transmitted from liquid to solid phase and *vice versa* and boosted its accuracy. This platform maintained the 82% of fluorescence intensity after 10 uses and the 85% of mechanical performance after 3 uses. Besides, it exhibited antibacterial properties and reduced about 93% and 96% of *E. coli* number after 1 d and 2 d, respectively. This sensor was capable of Cu^{2+} recognition in only neutral and alkaline solutions. Another sensor with adsorption properties was produced by Guo et al., 2019a, 2019b-through embedding CQD into carboxy-methylated CNF (CM-CNF) in the form of hydrogel. This hydrogel was able to adsorb several HMIs (Ba^{3+}, Pb^{3+}, Cu^{3+} and Fe^{3+}) whereas able to sense solely Fe^{3+} with fast visual response and the LOD of 18 mg L^{-1}. In this platform, the incorporation of CNF facilitated HMIs adsorption because of the existence of high density of carboxyl, hydroxyl and amide groups on its surface.

On the other hand, several hydrogels and aerogels have been developed for both detection and adsorption of Cr^{3+}/Cu^{6+} based on CNFs and CQDs. In these platforms, CNFs, capable of forming 3D structure readily and enhancing HMIs adsorption, acts as a template, and CQDs works as a sensing material due to its favorable fluorescence feature (Yuan et al., 2020a, 2020b). One of such sensors employed for Cr^{3+} detection was devised by Song et al. (2020) via a green process. In this sensor, cellulose was applied as a carbon sources for preparing CQDs through hydrothermal method, and no hazardous byproducts were produced. It should be noted that this sensing platform did not lose its efficiency in strong acidic media although some active sites were occupied by H^{+} instead of Cr^{3+}. Yuan et al. (2020b)prepared an aerogel based on CQD and CM-CNF, isolated from bleached eucalyptus kraft pulp, identifying Cr^{6+} with 17.6 mg L-1 LOD. The preparation process of the aerogel is depicted in Fig. 5a. This sensor showed satisfactory selectivity and sensitivity towards this HMI. As can be seen in Fig. 5b, among various ions, Cr^{6+} ended in the most obvious fluorescence quenching due to its robust electron capturing capability and more electron transfer between Cr^{6+} and CQD.

On the other hand, Fig. 5c displays that the increase in Cr^{6+} concentration caused the fluorescence color to turn from bright blue into dark black. In another work, Yuan et al. (2021) manufactured a hydrogel for Cr^{6+} diagnosis whose LOD was lower than the aerogel in their previous work (11.2 mg L^{-1}) (Yuan et al., 2020a, 2020b). They utilized wood bleached pulp as an initial substance and incorporated TOCNF and CQD into lignin-based hydrogels (Fig. 5d) (Yuan et al., 2021). The selectivity and sensitivity of this hydrogel were estimated by doing experiments in the presence of interfering HMIs and varying concentrations of Cr^{6+}, respectively. The results are shown in Fig. 5e, f. Another fluorescent adsorbing and sensing platform for Cr^{6+} was developed by Luo et al. (2021) through the incorporation of TOCNF modified with

[1] PA6 containing CNW/Ag in the bulk.
[2] PA6 coated with CNW: Ag.
[3] PA6/CNW coated with AgNPs.

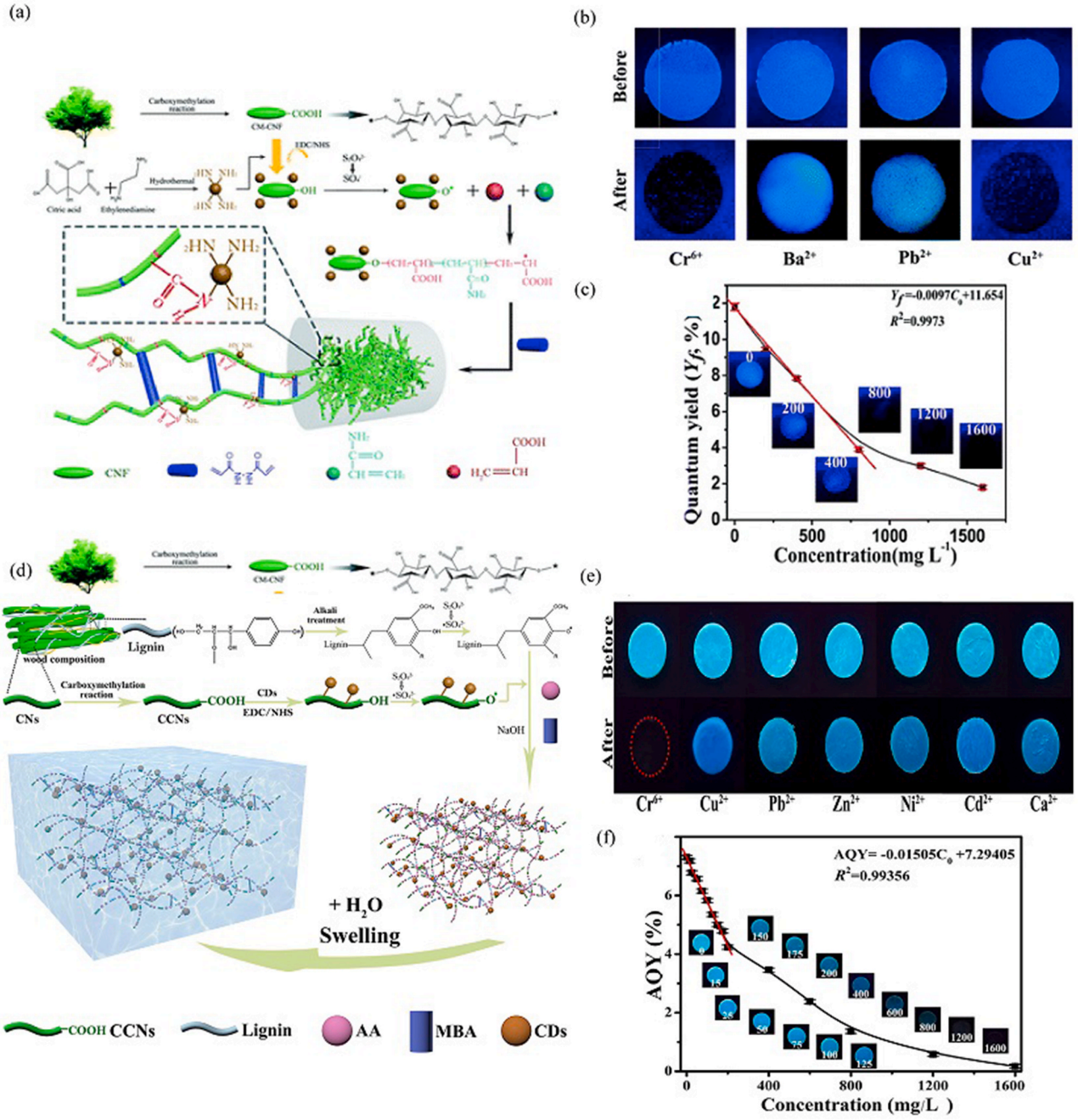

Fig. 5. a) Synthesis procedure of aerogel. b) Effect of various HMIs at the concentration of 10^3 mg L^{-1} on fluorescence quenching. c) Effect of increase in Cr^{6+} concentration on fluorescence quenching (Yuan et al., 2020a, 2020b). d) Synthesis rout of hydrogel. e) Effect of various HMIs at the concentration of 2×10^3 mg L^{-1} on fluorescence quenching. f) Gradual decrease in fluorescence with increase in Cr^{6+} concentration (Yuan et al., 2021).

CQD and titanate (TN) into chitosan-based hydrogel. The utilization of TN alongside the TOCNF boosted the adsorption performance because of its porous structure which was confirmed by FTIR and XPS. In fact, the porous structure of TOCNF engendered numbers of active sites and channels for analytes transportation, which improved the adsorption and binding events between analytes and receptors, hence stabilized fluorescence signal and enhanced the detection. The LOD and linear range of detection of this sensor were calculated 8.5 and 10–80 mg L^{-1}, respectively. In all these studies undertaken on Cr^{6+} detection in water, the presence of amino groups on the surface of CQD was conducive to adsorbing Cr^{6+} because of electrostatic attraction between them. Furthermore, some of Cr^{6+} ions, which were reduced to Cr^{3+}, formed complexes with hydroxyl, carboxyl and amino functional groups. In this way, this HMI was detectable by the suggested sensors (Kumeria, 2015; Luo et al., 2021; Yuan et al., 2020a, 2020b, 2021). The summary of different dimensional nanocellulose-based sensors devised for HMIs detection is listed in Table 2.

5. Conclusions

Nanocellulose-based platforms are novel approaches to manufacture renewable, efficient, low cost, optical and/or electrochemical analytical devices in the forms of nanofibers, films and also gel like materials for (bio)sensing applications. It is evidence that, CNC, CNF and BC, different sorts of nanocellulose are highly regarded for the fabrication of sensing platforms functioning on a basis of fluorescence, SPR, structural

Table 2
Summary of HMIs sensors based on different dimensional NC.

Sensor category	Sensing function		Sensing platform	HMI	NC type	NC role	Sensing material	Response range/ LOD	Ref.
1D	Optical	Fluorescent	AANI-labeled TOCNC	Pb^{2+}	CNC	Carrier	AANI and TOCNC	0.15–50 μM/0.15 μM	Song et al. (2019)
			Py-CNC	Fe^{3+}	CNC	Matrix	Py	1–200 μM/1 μM	Zhang et al. (2012)
		SPR	CNW/AuNP	Cd^{2+}	CNW	Dispersant	AuNPs	500–2000 nM/60 nM	Migliorini et al. (2020)
		Fluorescent Colorimetric	SNS-DETA	Cu^{2+}	SNC	Matrix	DETA	N.D. [1] 100–150 mg L^{-1}	Ram et al. (2020)
		Fluorescent Colorimetric	SNC-DETA-EA					1.03 mg L^{-1} 0.5–100 mg L^{-1}/0.5 mg L^{-1}	
		Fluorescent Colorimetric	RhB–CNC	Hg^{2+}	CNC	Matrix	RhB	232 nM 746 nM	Ye et al. (2020)
		Fluorescent Colorimetric	TOCNF-DA	Fe^{3+}	CNF	Matrix	DA	6.6 × 10^{-11} M 5 × 10^{-7} M	Wang et al. (2020b)
2D	Optical	Fluorescent	TOCNF-CQD	Fe^{3+}	CNF	Substrate	CQD	10–1000 μM	Xue et al. (2020)
			BC/N-CQD	Fe^{3+}	BC	Substrate	N-CQD	0.5–600 μM/84 μM	Lv et al. (2017)
			BC/N-GOQD	Fe^{3+}	BC	Matrix	N-GOQD	0.5–650 μM/69 nM	Lv et al. (2019)
			TOCNF/3,5-BHNMABA	Cu^{2+} Cs^{2+}	CNF	Matrix	3,5-BHNMABA	10–600 mg L^{-1}	Rahmawati et al. (2020)
		SPR	CTA-CNC/GO	Cu^{2+}	CNC	Matrix	GO	0.01–0.5 mg L^{-1}/ 0.01 mg L-1	(Daniyal et al., 2018a, 2018b, 2018a)
				Ni^{2+}				0.01–0.1 mg L^{-1}/ 0.01 mg L^{-1}	Daniyal et al. (2019a)
				Zn^{2+}				0.01–0.1 mg L^{-1}/ 0.01 mg L^{-1}	Daniyal et al. (2019b)
			CNC-GO	Cu^{2+} Zn^{2+}				N.D.	Daniyal et al. (2020)
			RhB-BC	Cu^{2+}	BC		RhB	N.D.	Milindanuth and Pisitsak (2018)
	Electro-chemical	Voltammetric	SnO_2-BC	Ni^{2+}	BC	Matrix	SnO_2	N.D.	Sakwises et al. (2017)
			TONFC/GCE	Cd^{2+}	NFC		TONFC	5 nM	Zinoubi et al. (2017)
				Cu^{2+}				0.5 nM	
				Pb^{2+}				0.5 nM	
				Hg^{2+}				5 nM	
			DPA-NC/PGE	Cu^{2+}	N.D.		DPA	0.2–50 pM/0.048 pM	Taheri et al. (2018)
			γ-AlOOH-CBC/ GCE	Cd^{2+}	BC	Carrier	γ-AlOOH	0.5–250 μg L^{-1}/ 0.17 μg L^{-1}	Qin et al. (2018)
				Pb^{2+}				0.5–250 μg L^{-1}/0.1 μg L^{-1}	
			PA6/CNW/rGO	Hg^{2+}	CNW	Reducing agent	PA6	2.5–200 μM/0.0052 μM	Teodoro et al. (2019a)
		Impedimetric	E− tongue	Cd^{2+}	CNW	stabilizing agent	Ag NPs	N.D.	Teodoro et al. (2019b)
				Cu^{2+}				N.D.	
				Ni^{2+}				N.D.	
				Pb^{2+}				10 nM	
3D	Optical	Fluorescent	Au@BSA NCs–CNC-ALG	Hg^{2+}	CNC	Substrate	Au@BSA NCs	N.D.	Mohammed et al. (2016)
			BSA- Au NCs/ TOCNC	Hg^{2+}	CNC	Substrate	BSA- Au NCs	5–150 mg L^{-1}/2.7 mg L^{-1}	Lei et al. (2021)
			PVA/borax-TOCNF/ST	Cu^{2+}	CNF	Dispersant	ST	0.1–10 μM/0.086 μM	Yue et al. (2021)
			CQD/CM-CNF	Fe^{3+}	CNF	Template	CQD	18 mg L^{-1}	Song et al. (2020)
			CQD/CNF	Cr^{3+}	CNF	Template	CQD	N.D.	Song et al. (2020)
			CQD/CM-CNF	Cr^{6+}				17.6 mg L^{-1}	Yuan et al. (2020)
			Lignin/CQD/ TOCNF					11.2 mg L^{-1}	Yuan et al. (2021)
			CS/TN/CQD/ TOCNF					10–80 mg L^{-1}/8.5 mg L^{-1}	Luo et al. (2021)

1. not described.

colorimetric and conductive responses for HMIs diagnosis. It is noteworthy to mention that 3D structure of nanocellulose made it an extremely desirable choice for making hydrogels and aerogels with fluorescent characteristics inasmuch as its porous structure provides receptor with large surface area culminating in the more interaction between analyte and receptor. Additionally, the presence of hydroxyl groups on the surface of such biopolymers have brought them the opportunity of being functionalized with NPs (plasmonic NPs and photoluminescent nanodots), macromolecules and dyes through which they are capable of forming complex with HMIs and detecting them.

Overall, we believe that the progress in nanocellulose-based sensors will lead to the development of much more practical sensors that will substitute conventional ones.

Credit

Mahsa Mousavi Langari: Visualization, Writing – original draft; **M. Mirari Antxustegi:** Supervision, Writing – review & editing, **Jalel Labidi:** Conceptualization; Writing – review & editing.

Declaration of competing interest

The authors declare that they have no known competing financial interests or personal relationships that could have appeared to influence the work reported in this paper.

Acknowledgements

The authors would like to thank the University of the Basque Country (Training of Researcher Staff, PIF 20/197).

References

Ababneh, F.A., Al-Momani, I.F., 2018. Assessments of toxic heavy metals contamination in cosmetic products. Environ. Forensics 19, 134–142. https://doi.org/10.1080/15275922.2018.1448908.

Abitbol, T., Rivkin, A., Cao, Y., Nevo, Y., Abraham, E., Ben-Shalom, T., Lapidot, S., Shoseyov, O., 2016. Nanocellulose, a tiny fiber with huge applications. Curr. Opin. Biotechnol. 39, 76–88. https://doi.org/10.1016/j.copbio.2016.01.002.

Ahankari, S., George, T., Subhedar, A., Kar, K.K., 2020. Nanocellulose as a sustainable material for water purification. SPE Polym. 1, 69–80. https://doi.org/10.1002/pls2.10019.

Aliheidari, N., Aliahmad, N., Agarwal, M., Dalir, H., 2019. Electrospun nanofibers for label-free sensor applications. Sensors 19. https://doi.org/10.3390/s19163587.

Anirudhan, T.S., Deepa, J.R., Binussreejayan, 2018. Electrochemical sensing of cholesterol by molecularly imprinted polymer of silylated graphene oxide and chemically modified nanocellulose polymer. Mater. Sci. Eng. C 92, 942–956. https://doi.org/10.1016/j.msec.2018.07.041.

Bacakova, L., Pajorova, J., Bacakova, M., Skogberg, A., Kallio, P., Kolarova, K., Svorcik, V., 2019. Versatile application of nanocellulose: from industry to skin tissue engineering and wound healing. Nanomaterials 9. https://doi.org/10.3390/nano9020164.

Bacakova, L., Pajorova, J., Tomkova, M., Matejka, R., Broz, A., Stepanovska, J., Prazak, S., Skogberg, A., Siljander, S., Kallio, P., 2020. Applications of nanocellulose/nanocarbon composites: focus on biotechnology and medicine. Nanomaterials 10, 1–32. https://doi.org/10.3390/nano10020196.

Balusamy, B., Senthamizhan, A., Uyar, T., 2020. Functionalized electrospun nanofibers as a versatile platform for colorimetric detection of heavy metal ions in water: a review. Materials 13. https://doi.org/10.3390/ma13102421.

Bergmann, E., 1932. Communications to the editor. J. Am. Chem. Soc. 54, 3773–3782. https://doi.org/10.1021/ja01348a044.

Brett, C.J., Mittal, N., Ohm, W., Gensch, M., Kreuzer, L.P., Körstgens, V., Månsson, M., Frielinghaus, H., Müller-Buschbaum, P., Söderberg, L.D., Roth, S.V., 2019. Water-Induced structural rearrangements on the nanoscale in ultrathin nanocellulose films. Macromolecules. https://doi.org/10.1021/acs.macromol.9b00531.

Briffa, J., Sinagra, E., Blundell, R., 2020. Heavy metal pollution in the environment and their toxicological effects on humans. Heliyon 6, e04691. https://doi.org/10.1016/j.heliyon.2020.e04691.

Carlsson, D.O., Nyström, G., Zhou, Q., Berglund, L.A., Nyholm, L., Stromme, M., 2012. Electroactive nanofibrillated cellulose aerogel composites with tunable structural and electrochemical properties. J. Mater. Chem. 22, 19014–19024. https://doi.org/10.1039/c2jm33975g.

Cemple, M., Nikel, G., 2006. Nickel: a review of its sources and environmental toxicology. Pol. J. Environ. Stud. 15.

Chen, H., Huang, J., Hao, B., Yang, B., Chen, S., Yang, G., Xu, J., 2019. Citrate-based fluorophore-modified cellulose nanocrystals as a biocompatible fluorescent probe for detecting ferric ions and intracellular imaging. Carbohydr. Polym. 224, 115198. https://doi.org/10.1016/j.carbpol.2019.115198.

Cheng, H., Du, Y., Wang, B., Mao, Z., Xu, H., Zhang, L., Zhong, Y., Jiang, W., Wang, L., Sui, X., 2018. Flexible cellulose-based thermoelectric sponge towards wearable pressure sensor and energy harvesting. Chem. Eng. J. 338, 1–7. https://doi.org/10.1016/j.cej.2017.12.134.

Chillawar, R.R., Tadi, K.K., Motghare, R.V., 2015. Voltammetric techniques at chemically modified electrodes. J. Anal. Chem. 70, 399–418. https://doi.org/10.1134/S1061934815040152.

Daniyal, W.M.E.M.M., Fen, Y.W., Abdullah, J., Sadrolhosseini, A.R., Saleviter, S., Omar, N.A.S., 2018a. Exploration of surface plasmon resonance for sensing copper ion based on nanocrystalline cellulose-modified thin film. Opt Express 26, 34880. https://doi.org/10.1364/oe.26.034880.

Daniyal, W.M.E.M.M., Fen, Y.W., Abdullah, J., Saleviter, S., Sheh Omar, N.A., 2018b. Preparation and characterization of hexadecyltrimethylammonium bromide modified nanocrystalline cellulose/graphene oxide composite thin film and its potential in sensing copper ion using surface plasmon resonance technique. Optik 173, 71–77. https://doi.org/10.1016/j.ijleo.2018.08.014.

Daniyal, W.M.E.M.M., Fen, Y.W., Abdullah, J., Sadrolhosseini, A.R., Saleviter, S., Omar, N.A.S., 2019a. Label-free optical spectroscopy for characterizing binding properties of highly sensitive nanocrystalline cellulose-graphene oxide based nanocomposite towards nickel ion. Spectrochim. Acta, Part A 212, 25–31. https://doi.org/10.1016/j.saa.2018.12.031.

Daniyal, W.M.E.M.M., Fen, Y.W., Anas, N.A.A., Omar, N.A.S., Ramdzan, N.S.M., Nakajima, H., Mahdi, M.A., 2019b. Enhancing the sensitivity of a surface plasmon resonance-based optical sensor for zinc ion detection by the modification of a gold thin film. RSC Adv. 9, 41729–41736. https://doi.org/10.1039/c9ra07368j.

Daniyal, W.M.E.M.M., Fen, Y.W., Abdullah, J., Hashim, H.S., Fauzi, N., Illya, M., Chanlek, N., Mahdi, M.A., 2020. X-ray photoelectron study on gold/nanocrystalline cellulose-graphene oxide thin film as surface plasmon resonance active layer for metal ion detection. Thin Solid Films 713, 138340. https://doi.org/10.1016/j.tsf.2020.138340.

De France, K., Zeng, Z., Wu, T., Nyström, G., 2020. Functional materials from nanocellulose: utilizing structure–property relationships in bottom-up fabrication. Adv. Mater. 2000657. https://doi.org/10.1002/adma.202000657.

Dwivedi, A.D., Dubey, S.P., Hokkanen, S., Sillanpää, M., 2014. Mechanistic investigation on the green recovery of ionic, nanocrystalline, and metallic gold by two anionic nanocelluloses. Chem. Eng. J. 253, 316–324. https://doi.org/10.1016/j.cej.2014.05.069.

Fan, X., White, I.M., Shopova, S.I., Zhu, H., Suter, J.D., Sun, Y., 2008. Sensitive optical biosensors for unlabeled targets: a review. Anal. Chim. Acta 620, 8–26. https://doi.org/10.1016/j.aca.2008.05.022.

Fan, J., Zhang, S., Li, F., Shi, J., 2020. Cellulose-based Sensors for Metal Ions Detection. Cellulose. Springer Netherlands. https://doi.org/10.1007/s10570-020-03158-x.

Farooq, Amjad, Patoary, M.K., Zhang, M., Mussana, H., Li, M., Naeem, M.A., Mushtaq, M., Farooq, Aamir, Liu, L., 2020. Cellulose from sources to nanocellulose and an overview of synthesis and properties of nanocellulose/zinc oxide nanocomposite materials. Int. J. Biol. Macromol. 154, 1050–1073. https://doi.org/10.1016/j.ijbiomac.2020.03.163.

Fiel, W.A., Freitas Borges, P.A. de, Cunha Lins, V. de F., Dorledo de Faria, R.A., 2019. Recent advances on the electrochemical transduction techniques for the biosensing of pharmaceuticals in aquatic environments. Int. J. Biosens. Bioelectron. 5, 119–123. https://doi.org/10.15406/ijbsbe.2019.05.00164.

Fu, Z., Xi, S., 2020. The effects of heavy metals on human metabolism. Toxicol. Mech. Methods 30, 167–176. https://doi.org/10.1080/15376516.2019.1701594.

Geană, E.I., Ciucure, C.T., Apetrei, C., 2020. Electrochemical sensors coupled with multivariate statistical analysis as screening tools for wine authentication issues: a review. Chemosensors 8. https://doi.org/10.3390/CHEMOSENSORS8030059.

Genchi, G., Carocci, A., Lauria, G., Sinicropi, M.S., Catalano, A., 2020. Nickel: human health and environmental toxicology. Int. J. Environ. Res. Publ. Health 17. https://doi.org/10.3390/ijerph17030679.

Golmohammadi, H., Morales-narváez, E., Naghdi, T., Merkoçi, A., 2017. Nanocellulose in (Bio) Sensing Nanocellulose in (Bio) Sensing.

Gómez-Ariza, J.L., Lorenzo, F., García-Barrera, T., 2005. Comparative study of atomic fluorescence spectroscopy and inductively coupled plasma mass spectrometry for mercury and arsenic multispeciation. Anal. Bioanal. Chem. 382, 485–492. https://doi.org/10.1007/s00216-005-3094-7.

Gong, S., Cheng, W., 2017. One-dimensional nanomaterials for soft electronics. Adv. Electron. Mater. 3 https://doi.org/10.1002/aelm.201600314.

Gumpu, M.B., Sethuraman, S., Krishnan, U.M., Rayappan, J.B.B., 2015. A review on detection of heavy metal ions in water - an electrochemical approach. Sens. Actuators, B 213, 515–533. https://doi.org/10.1016/j.snb.2015.02.122.

Guo, W., He, H., Zhu, H., Hou, X., Chen, X., Zhou, S., Wang, S., Huang, L., Lin, J., 2019a. Preparation and properties of a biomass cellulose-based colorimetric sensor for Ag^{+} and Cu^{2+}. Ind. Crop. Prod. 137, 410–418. https://doi.org/10.1016/j.indcrop.2019.05.044.

Guo, X., Xu, D., Yuan, H., Luo, Q., Tang, S., Liu, L., Wu, Y., 2019b. A novel fluorescent nanocellulosic hydrogel based on carbon dots for efficient adsorption and sensitive sensing in heavy metals. J. Mater. Chem. 7, 27081–27088. https://doi.org/10.1039/c9ta11502a.

Gupta, G.K., Shukla, P., 2020. Lignocellulosic biomass for the synthesis of nanocellulose and its eco-friendly advanced applications. Front. Chem. 8 https://doi.org/10.3389/fchem.2020.601256.

Hasan, M., Salam, A., Alam, A.M.S., 2009. Identification and characterization of trace metals in black solid materials deposited from biomass burning at the cooking stoves in Bangladesh. Biomass Bioenergy 33, 1376–1380. https://doi.org/10.1016/j.biombioe.2009.05.023.

Hasanpour, M., Hatami, M., 2020. Application of three dimensional porous aerogels as adsorbent for removal of heavy metal ions from water/wastewater: a review study. Adv. Colloid Interface Sci. 284, 102247. https://doi.org/10.1016/j.cis.2020.102247.

Hu, D., Ma, W., Zhang, Z., Ding, Y., Wu, L., 2020. Dual bio-inspired design of highly thermally conductive and superhydrophobic nanocellulose composite films. ACS Appl. Mater. Interfaces. https://doi.org/10.1021/acsami.0c01425.

Huang, H., Ge, H., Ren, Z., Huang, Z., Xu, M., Wang, X., 2021. Controllable synthesis of biocompatible fluorescent carbon dots from cellulose hydrogel for the specific detection of Hg^{2+}. Front. Bioeng. Biotechnol. 9, 1–10. https://doi.org/10.3389/fbioe.2021.617097.

Islam, M.N., Channon, R.B., 2019. Electrochemical Sensors, Bioengineering Innovative Solutions for Cancer. Elsevier Ltd. https://doi.org/10.1016/B978-0-12-813886-1.00004-8.

Ivanova, N., Gugleva, V., Dobreva, M., Pehlivanov, I., Stefanov, S., Andonova, V., 2016. We Are IntechOpen , the World ' S Leading Publisher of Open Access Books Built by Scientists , for Scientists TOP 1 %. Intech i, p. 13.

Jiang, X., Xia, J., Luo, X., 2020. Simple, rapid, and highly sensitive colorimetric sensor strips from a porous cellulose membrane stained with victoria blue B for efficient detection of trace Cd(II) in water. ACS Sustain. Chem. Eng. 8, 5184–5191. https://doi.org/10.1021/acssuschemeng.9b07614.

Karuk Elmas, S.N., Dincer, Z.E., Erturk, A.S., Bostanci, A., Karagoz, A., Koca, M., Sadi, G., Yilmaz, I., 2020. A novel fluorescent probe based on isocoumarin for Hg^{2+} and Fe^{3+}

ions and its application in live-cell imaging. Spectrochim. Acta, Part A 224, 117402. https://doi.org/10.1016/j.saa.2019.117402.
Khan, Z.G., Patil, P.O., 2020. A comprehensive review on carbon dots and graphene quantum dots based fluorescent sensor for biothiols. Microchem. J. 157, 105011. https://doi.org/10.1016/j.microc.2020.105011.
Khansili, N., Rattu, G., Krishna, P.M., 2018. Label-free optical biosensors for food and biological sensor applications. Sens. Actuators, B 265, 35–49. https://doi.org/10.1016/j.snb.2018.03.004.
Kinuthia, G.K., Ngure, V., Beti, D., Lugalia, R., Wangila, A., Kamau, L., 2020. Levels of heavy metals in wastewater and soil samples from open drainage channels in Nairobi, Kenya: community health implication. Sci. Rep. 10, 1–13. https://doi.org/10.1038/s41598-020-65359-5.
Koga, H., Nagashima, K., Huang, Y., Zhang, G., Wang, C., Takahashi, T., Inoue, A., Yan, H., Kanai, M., He, Y., Uetani, K., Nogi, M., Yanagida, T., 2019. Paper-based disposable molecular sensor constructed from oxide nanowires, cellulose nanofibers, and pencil-drawn electrodes. ACS Appl. Mater. Interfaces 11, 15044–15050. https://doi.org/10.1021/acsami.9b01287.
Kumeria, T., 2015. Development of Nanopore Based Label-free Optical Sensors Tushar Kumeria.
Lei, X., Li, H., Luo, Y., Sun, X., Guo, X., Hu, Y., Wen, R., 2021. Novel fluorescent nanocellulose hydrogel based on gold nanoclusters for the effective adsorption and sensitive detection of mercury ions. J. Taiwan Inst. Chem. Eng. 123, 79–86. https://doi.org/10.1016/j.jtice.2021.05.044.
Lesani, P., Singh, G., Viray, C.M., Ramaswamy, Y., Zhu, D.M., Kingshott, P., Lu, Z., Zreiqat, H., 2020. Two-photon dual-emissive carbon dot-based brobe: deep-tissue imaging and ultrasensitive sensing of intracellular ferric ions. ACS Appl. Mater. Interfaces 12, 18395–18406. https://doi.org/10.1021/acsami.0c05217.
Li, Z.X., Guo, Y.A., 2005. Simultaneous determination of trace arsenic, antimony, bismuth and selenium in biological samples by hydride generation-four-channel atomic fluorescence spectrometry. Talanta 65, 1318–1325. https://doi.org/10.1016/j.talanta.2004.09.021.
Li, B., Mei, H., Chang, Y., Xu, K., Yang, L., 2020. A novel near-infrared turn-on fluorescent probe for the detection of Fe^{3+} and Al^{3+} and its applications in living cells imaging. Spectrochim. Acta, Part Athin film 239, 118552. https://doi.org/10.1016/j.saa.2020.118552.
Lokhande, R.S., Singare, P.U., Pimple, D.S., 2011. Toxicity study of heavy metals pollutants in waste water effluent samples collected from Taloja Industrial Estate of Mumbai, India. Resour. Environ. 1, 13–19.
Lu, Y., Liang, X., Niyungeko, C., Zhou, J., Xu, J., Tian, G., 2018. A review of the identification and detection of heavy metal ions in the environment by voltammetry. Talanta 178, 324–338. https://doi.org/10.1016/j.talanta.2017.08.033.
Luo, Q., Huang, X., Luo, Y., Yuan, H., Ren, T., Li, X., Xu, D., Guo, X., Wu, Y., 2021. Fluorescent chitosan-based hydrogel incorporating titanate and cellulose nanofibers modified with carbon dots for adsorption and detection of Cr(VI). Chem. Eng. J. 407, 127050. https://doi.org/10.1016/j.cej.2020.127050.
Lv, P., Yao, Y., Li, D., Zhou, H., Naeem, M.A., Feng, Q., Huang, J., Cai, Y., Wei, Q., 2017. Self-assembly of nitrogen-doped carbon dots anchored on bacterial cellulose and their application in iron ion detection. Carbohydr. Polym. 172, 93–101. https://doi.org/10.1016/j.carbpol.2017.04.086.
Lv, P., Zhou, H., Mensah, A., Feng, Q., Lu, K., Huang, J., Li, D., Cai, Y., Lucia, L., Wei, Q., 2019. In situ 3D bacterial cellulose/nitrogen-doped graphene oxide quantum dot-based membrane fluorescent probes for aggregation-induced detection of iron ions. Cellulose 26, 6073–6086. https://doi.org/10.1007/s10570-019-02476-z.
Malik, L.A., Bashir, A., Qureashi, A., Pandith, A.H., 2019. Detection and removal of heavy metal ions: a review. Environ. Chem. Lett. 17, 1495–1521. https://doi.org/10.1007/s10311-019-00891-z.
Manzoor, M.M., 2020. Environmental biotechnology: for sustainable future. Bioremed. Biotechnol. 2 https://doi.org/10.1007/978-3-030-40333-1_14.
Mayr, T., Wolfbeis, O.S., 2002. Optical Sensors for the Determination of Heavy Metal Ions Ph.D. Thes, p. 140.
Migliorini, F.L., Teodoro, K.B.R., Correa, D.S., 2020. Green-synthesized gold nanoparticles supported on cellulose nanowhiskers for easy-to-interpret colorimetric detection of cadmium (II). Cellul. Chem. Technol. 54, 407–411. https://doi.org/10.35812/CelluloseChemTechnol.2020.54.41.
Milindanuth, P., Pisitsak, P., 2018. A novel colorimetric sensor based on rhodamine-B derivative and bacterial cellulose for the detection of Cu(II) ions in water. Mater. Chem. Phys. 216, 325–331. https://doi.org/10.1016/j.matchemphys.2018.06.003.
Mohammed, N., Baidya, A., Murugesan, V., Kumar, A.A., Ganayee, M.A., Mohanty, J.S., Tam, K.C., Pradeep, T., 2016. Diffusion-controlled simultaneous sensing and scavenging of heavy metal ions in water using atomically precise cluster-cellulose nanocrystal composites. ACS Sustain. Chem. Eng. 4, 6167–6176. https://doi.org/10.1021/acssuschemeng.6b01674.
Muhd Julkapli, N., Bagheri, S., 2017. Nanocellulose as a green and sustainable emerging material in energy applications: a review. Polym. Adv. Technol. 28, 1583–1594. https://doi.org/10.1002/pat.4074.
Neubauerova, K., Carneiro, M.C.C.G., Rodrigues, L.R., Moreira, F.T.C., Sales, M.G.F., 2020. Nanocellulose- based biosensor for colorimetric detection of glucose. Sens. Bio-Sens. Res. 29, 100368. https://doi.org/10.1016/j.sbsr.2020.100368.
Ojha, A., 2020. Materials in electrochemical detection of water pollutants. https://doi.org/10.1007/978-981-15-0671-0_10.
Omran, A.A.B., Mohammed, A.A.B.A., Sapuan, S.M., Ilyas, R.A., Asyraf, M.R.M., Koloor, S.S.R., Petrů, M., 2021. Micro-and nanocellulose in polymer composite materials: a review. Polymers 13, 1–30. https://doi.org/10.3390/polym13020231.
Phichi, M., Imyim, A., Tuntulani, T., Aeungmaitrepirom, W., 2020. Paper-based cation-selective optode sensor containing benzothiazole calix[4]arene for dual colorimetric Ag^{+} and Hg^{2+} detection. Anal. Chim. Acta 1104, 147–155. https://doi.org/10.1016/j.aca.2020.01.005.
Piras, C.C., Fernández-Prieto, S., De Borggraeve, W.M., 2019. Ball milling: a green technology for the preparation and functionalisation of nanocellulose derivatives. Nanoscale Adv. 1, 937–947. https://doi.org/10.1039/c8na00238j.
Pursula, P., Kiri, K., Caffrey, C.M., Sandberg, H., Vartiainen, J., Flak, J., Lahtinen, P., 2018. Nanocellulose-polyurethane substrate material with tunable mechanical properties for wearable electronics. Flex. Print. Electron. 3 https://doi.org/10.1088/2058-8585/aae5d9.
Qin, D., Hu, X., Dong, Y., Mamat, X., Li, Y., Wågberg, T., Hu, G., 2018. An electrochemical sensor based on green γ-AlOOH-carbonated bacterial cellulose hybrids for simultaneous determination trace levels of Cd(II) and Pb(II) in drinking water. J. Electrochem. Soc. 165, B328–B334. https://doi.org/10.1149/2.1321807jes.
Raghav, N., Sharma, M.R., Kennedy, J.F., 2021. Nanocellulose: a mini-review on types and use in drug delivery systems. Carbohydr. Polym. Technol. Appl. 2, 100031. https://doi.org/10.1016/j.carpta.2020.100031.
Rahmawati, A., Shih, C.F., Imae, T., 2020. Film sensor of a ligand-functionalized cellulose nanofiber for the selective detection of copper and cesium ions. Polym. J. 52, 1235–1243. https://doi.org/10.1038/s41428-020-0377-y.
Ram, B., Jamwal, S., Ranote, S., Chauhan, G.S., Dharela, R., 2020. Highly selective and rapid naked-eye colorimetric sensing and fluorescent studies of Cu^{2+} ions derived from spherical nanocellulose. ACS Appl. Polym. Mater. 2, 5290–5299. https://doi.org/10.1021/acsapm.0c01025.
Ramdzan, N.S.M., Fen, Y.W., Anas, N.A.A., Omar, N.A.S., Saleviter, S., 2020. Development of biopolymer and conducting polymer-based optical sensors for heavy metal ion detection. Molecules 25. https://doi.org/10.3390/molecules25112548.
Rezvani, S.A., Soleymanpour, A., 2016. Application of l-cystine modified zeolite for preconcentration and determination of ultra-trace levels of cadmium by flame atomic absorption spectrometry. J. Chromatogr. A 1436, 34–41. https://doi.org/10.1016/j.chroma.2016.01.065.
Riva, L., Fiorati, A., Sganappa, A., Melone, L., Punta, C., Cametti, M., 2019. Naked-eye heterogeneous sensing of fluoride ions by co-polymeric nanosponge systems comprising aromatic-imide-functionalized nanocellulose and branched polyethyleneimine. Chempluschem 84, 1512–1518. https://doi.org/10.1002/cplu.201900348.
Rodríguez-Méndez, M.L., Apetrei, C., De Saja, J.A., 2010. Electronic Tongues Purposely Designed for the Organoleptic Characterization of Olive Oils, Olives and Olive Oil in Health and Disease Prevention. Elsevier Inc. https://doi.org/10.1016/B978-0-12-374420-3.00057-7.
Ruiz-Palomero, C., Soriano, M.L., Valcárcel, M., 2016. Gels based on nanocellulose with photosensitive ruthenium bipyridine moieties as sensors for silver nanoparticles in real samples. Sens. Actuators, B 229, 31–37. https://doi.org/10.1016/j.snb.2016.01.098.
Ružičková, S., Remeteiová, D., Mičková, V., Dirner, V., 2018. Sediment matrix characterization as a tool for evaluating the environmental impact of heavy metals in metal mining, smelting, and ore processing areas. Environ. Monit. Assess. 190 https://doi.org/10.1007/s10661-018-6551-4.
Sakwises, L., Rodthongkum, N., Ummartyotin, S., 2017. SnO2- and bacterial-cellulose nanofiber-based composites as a novel platform for nickel-ion detection. J. Mol. Liq. 248, 246–252. https://doi.org/10.1016/j.molliq.2017.10.047.
Sang, S., Wang, Y., Feng, Q., Wei, Y., Ji, J., Zhang, W., 2016. Progress of new label-free techniques for biosensors: a review. Crit. Rev. Biotechnol. 36, 465–481. https://doi.org/10.3109/07388551.2014.991270.
Sarma, N. Sen, Dutta, P., Chakravarty, S., 2019. Sustainable Nanostructural Materials in Biosensor Application, Dynamics of Advanced Sustainable Nanomaterials and Their Related Nanocomposites at the Bio-Nano Interface. Elsevier Inc. https://doi.org/10.1016/B978-0-12-819142-2.00009-4.
Shen, L.L., Zhang, G.R., Li, W., Biesalski, M., Etzold, B.J.M., 2017. Modifier-free microfluidic electrochemical sensor for heavy-metal detection. ACS Omega 2, 4593–4603. https://doi.org/10.1021/acsomega.7b00611.
Shetti, N.P., Nayak, D.S., Reddy, K.R., Aminabhvi, T.M., 2018. Graphene-clay-based Hybrid Nanostructures for Electrochemical Sensors and Biosensors, Graphene-Based Electrochemical Sensors for Biomolecules: A Volume in Micro and Nano Technologies. Elsevier Inc. https://doi.org/10.1016/B978-0-12-815394-9.00010-8.
Sitko, R., Janik, P., Zawisza, B., Talik, E., Margui, E., Queralt, I., 2015. Green approach for ultratrace determination of divalent metal ions and arsenic species using total-reflection X-ray fluorescence spectrometry and mercapto-modified graphene oxide nanosheets as a novel adsorbent. Anal. Chem. 87, 3535–3542. https://doi.org/10.1021/acs.analchem.5b00283.
Sixto, A., Fiedoruk-Pogrebniak, M., Rosende, M., Cocovi-Solberg, D., Knochen, M., Miró, M., 2016. A mesofluidic platform integrating restricted access-like sorptive microextraction as a front end to ICP-AES for the determination of trace level concentrations of lead and cadmium as contaminants in honey. J. Anal. At. Spectrom. 31, 473–481. https://doi.org/10.1039/c5ja00387c.
Song, R., Zhang, Q., Chu, Y., Zhang, L., Dai, H., Wu, W., 2019. Fluorescent cellulose nanocrystals for the detection of lead ions in complete aqueous solution. Cellulose 26, 9553–9565. https://doi.org/10.1007/s10570-019-02760-y.
Song, Z., Chen, X., Gong, X., Gao, X., Dai, Q., Nguyen, T.T., Guo, M., 2020. Luminescent carbon quantum dots/nanofibrillated cellulose composite aerogel for monitoring adsorption of heavy metal ions in water. Opt. Mater. 100, 109642. https://doi.org/10.1016/j.optmat.2019.109642.
Soriano, M.L., Dueñas-Mas, M.J., 2018. Promising sensing platforms based on nanocellulose, pp. 273–301. https://doi.org/10.1007/5346_2018_26.

Taheri, M., Ahour, F., Keshipour, S., 2018. Sensitive and selective determination of Cu^{2+} at D-penicillamine functionalized nano-cellulose modified pencil graphite electrode. J. Phys. Chem. Solid. 117, 180–187. https://doi.org/10.1016/j.jpcs.2018.02.035.

Teodoro, K.B.R., Migliorini, F.L., Facure, M.H.M., Correa, D.S., 2019a. Conductive electrospun nanofibers containing cellulose nanowhiskers and reduced graphene oxide for the electrochemical detection of mercury(II). Carbohydr. Polym. 207, 747–754. https://doi.org/10.1016/j.carbpol.2018.12.022.

Teodoro, K.B.R., Shimizu, F.M., Scagion, V.P., Correa, D.S., 2019b. Ternary nanocomposites based on cellulose nanowhiskers, silver nanoparticles and electrospun nanofibers: use in an electronic tongue for heavy metal detection. Sens. Actuators, B 290, 387–395. https://doi.org/10.1016/j.snb.2019.03.125.

Thomas, P., Duolikun, T., Rumjit, N.P., Moosavi, S., Lai, C.W., Bin Johan, M.R., Fen, L.B., 2020. Comprehensive review on nanocellulose: recent developments, challenges and future prospects. J. Mech. Behav. Biomed. Mater. 110, 103884. https://doi.org/10.1016/j.jmbbm.2020.103884.

Torres, F.G., Troncoso, O.P., Gonzales, K.N., Sari, R.M., Gea, S., 2020. Bacterial cellulose-based biosensors. Med. Devices Sens. 3, 1–13. https://doi.org/10.1002/mds3.10102.

Tracey, C.T., Torlopov, M.A., Martakov, I.S., Vdovichenko, E.A., Zhukov, M., Krivoshapkin, P.V., Mikhaylov, V.I., Krivoshapkina, E.F., 2020. Hybrid cellulose nanocrystal/magnetite glucose biosensors. Carbohydr. Polym. 247, 116704. https://doi.org/10.1016/j.carbpol.2020.116704.

Tshikovhi, A., Mishra, S.B., Mishra, A.K., 2020. Nanocellulose-based composites for the removal of contaminants from wastewater. Int. J. Biol. Macromol. Elsevier B.V. https://doi.org/10.1016/j.ijbiomac.2020.02.221.

Uzuncar, S., Ozdogan, N., Ak, M., 2021. Enzyme-free detection of hydrogen peroxide with a hybrid transducing system based on sodium carboxymethyl cellulose, poly (3,4-ethylenedioxythiophene) and prussian blue nanoparticles. Anal. Chim. Acta 1172, 338664. https://doi.org/10.1016/j.aca.2021.338664.

Wang, H., Pei, Y., Qian, X., An, X., 2020a. Eu-metal organic framework@TEMPO-oxidized cellulose nanofibrils photoluminescence film for detecting copper ions. Carbohydr. Polym. 236, 116030. https://doi.org/10.1016/j.carbpol.2020.116030.

Wang, L., Zhu, H., Xu, G., Hou, X., He, H., Wang, S., 2020b. A biocompatible cellulose-nanofiber-based multifunctional material for Fe^{3+} detection and drug delivery. J. Mater. Chem. C 8, 11796–11804. https://doi.org/10.1039/d0tc02604b.

Xu, T., Dai, H., Jin, Y., 2020. Electrochemical sensing of lead(II) by differential pulse voltammetry using conductive polypyrrole nanoparticles. Microchim. Acta 187. https://doi.org/10.1007/s00604-019-4027-z.

Xue, B., Yang, Y., Tang, R., Sun, Y., Sun, S., Cao, X., Li, P., Zhang, Z., Li, X., 2020. One-step hydrothermal synthesis of a flexible nanopaper-based Fe^{3+} sensor using carbon quantum dot grafted cellulose nanofibrils. Cellulose 27, 729–742. https://doi.org/10.1007/s10570-019-02846-7.

Yan, X., Li, H., Li, Y., Su, X., 2014. Visual and fluorescent detection of acetamiprid based on the inner filter effect of gold nanoparticles on ratiometric fluorescence quantum dots. Anal. Chim. Acta 852, 189–195. https://doi.org/10.1016/j.aca.2014.09.008.

Yang, B., Ren, J., Wang, M., Luo, H., Cao, Y., 2019. Concentrations and chemical fractions of Cu, Zn, Cd, and Pb at ten metallurgical sites in China. Environ. Sci. Pollut. Res. 26, 3603–3611. https://doi.org/10.1007/s11356-018-3881-2.

Ye, X., Kang, Y., Zhou, J., 2020. Rhodamine labeled cellulose nanocrystals as selective "naked-eye" colorimetric and fluorescence sensor for Hg^{2+} in aqueous solutions. Cellulose 27, 5197–5210. https://doi.org/10.1007/s10570-020-03126-5.

Yeung, V., Miller, D.D., Rutzke, M.A., 2017. Atomic absorption spectroscopy, atomic emission spectroscopy, and Inductively Coupled Plasma-Mass Spectrometry. Food Anal. 129–150. https://doi.org/10.1007/978-3-319-45776-5_9.

Yoon, J., Cho, H.Y., Shin, M., Choi, H.K., Lee, T., Choi, J.W., 2020. Flexible electrochemical biosensors for healthcare monitoring. J. Mater. Chem. B 8, 7303–7318. https://doi.org/10.1039/d0tb01325k.

Yuan, B., Li, L., Murugadoss, V., Vupputuri, S., Wang, J., Alikhani, N., Guo, Z., 2020a. Nanocellulose-based composite materials for wastewater treatment and waste-oil remediation. ES Food Agrofor 41–52. https://doi.org/10.30919/esfaf0004.

Yuan, H., Yang, G., Luo, Q., Xiao, T., Zuo, Y., Guo, X., Xu, D., Wu, Y., 2020b. A 3D net-like structured fluorescent aerogel based on carboxy-methylated cellulose nanofibrils and carbon dots as a highly effective adsorbent and sensitive optical sensor of Cr(vi). Environ. Sci. Nano 7, 773–781. https://doi.org/10.1039/c9en01394f.

Yuan, H., Peng, J., Ren, T., Luo, Q., Luo, Y., Zhang, N., Huang, Y., Guo, X., Wu, Y., 2021. Novel fluorescent lignin-based hydrogel with cellulose nanofibers and carbon dots for highly efficient adsorption and detection of Cr(VI). Sci. Total Environ. 760, 143395. https://doi.org/10.1016/j.scitotenv.2020.143395.

Yue, Y., Gu, J., Han, J., Wu, Q., Jiang, J., 2021. Effects of cellulose/salicylaldehyde thiosemicarbazone complexes on PVA based hydrogels: portable, reusable, and high-precision luminescence sensing of Cu^{2+}. J. Hazard Mater. 401, 123798. https://doi.org/10.1016/j.jhazmat.2020.123798.

Zhang, Lingzhi, Li, Q., Zhou, J., Zhang, Lina, 2012. Synthesis and photophysical behavior of pyrene-bearing cellulose nanocrystals for Fe^{3+} sensing. Macromol. Chem. Phys. 213, 1612–1617. https://doi.org/10.1002/macp.201200233.

Zhang, M., Zhang, L., Tian, H., Lu, A., 2020a. Universal preparation of cellulose-based colorimetric sensor for heavy metal ion detection. Carbohydr. Polym. 236, 116037. https://doi.org/10.1016/j.carbpol.2020.116037.

Zhang, Y. nan, Sun, Y., Cai, L., Gao, Y., Cai, Y., 2020b. Optical fiber sensors for measurement of heavy metal ion concentration: a review. Meas. J. Int. Meas. Confed. 158, 107742. https://doi.org/10.1016/j.measurement.2020.107742.

Zhang, Z., Liu, G., Li, X., Zhang, S., Xingqiang, L., Wang, Y., 2020c. Design and synthesis of fluorescent nanocelluloses for sensing and bioimaging applications. Chempluschem 85, 487–502. https://doi.org/10.1002/cplu.201900746.

Zhao, T., Yao, Y., Wang, M., Chen, R., Yu, Y., Wu, F., Zhang, C., 2017. Preparation of MnO2-modified graphite sorbents from spent Li-ion batteries for the treatment of water contaminated by lead, cadmium, and silver. ACS Appl. Mater. Interfaces 9, 25369–25376. https://doi.org/10.1021/acsami.7b07882.

Zhu, H., Suter, J.D., Fan, X., 2010. Label-free optical ring resonator bio/chemical sensors, pp. 259–279. https://doi.org/10.1007/978-3-642-02827-4_10.

Zhu, J., Ke, Y., Dai, J., You, Q., Wu, L., Li, J., Guo, J., Xiang, Y., Dai, X., 2020. Topological insulator overlayer to enhance the sensitivity and detection limit of surface plasmon resonance sensor. Nanophotonics 9, 1941–1951. https://doi.org/10.1515/nanoph-2019-0439.

Zhu, P., Kuang, Y., Wei, Y., Li, F., Ou, H., Jiang, F., Chen, G., 2021. Electrostatic self-assembly enabled flexible paper-based humidity sensor with high sensitivity and superior durability. Chem. Eng. J. 404, 127105. https://doi.org/10.1016/j.cej.2020.127105.

Zinge, C., Kandasubramanian, B., 2020. Nanocellulose based biodegradable polymers. Eur. Polym. J. 133, 109758. https://doi.org/10.1016/j.eurpolymj.2020.109758.

Zinoubi, K., Majdoub, H., Barhoumi, H., Boufi, S., Jaffrezic-Renault, N., 2017. Determination of trace heavy metal ions by anodic stripping voltammetry using nanofibrillated cellulose modified electrode. J. Electroanal. Chem. 799, 70–77. https://doi.org/10.1016/j.jelechem.2017.05.039.